

Nucleus-electron correlation revising molecular bonding fingerprints from the exact wavefunction factorization

Ziyong Chen and Jun Yang^{a)}

Department of Chemistry

The University of Hong Kong, Hong Kong SAR, P.R. China

(Dated: 1 September 2021)

We present a novel theory and implementation for computing coupled electronic and quantal nuclear subsystems on a single potential energy surface, moving beyond the standard Born-Oppenheimer (BO) separation of nuclei and electrons. We formulate an exact self-consistent nucleus-electron embedding potential from the single product molecular wavefunction, and demonstrate that the fundamental behavior of correlated nucleus-electron can be computed for mean-field electrons that are responsive to a quantal anharmonic vibration of selected nuclei in a discrete variable representation. Geometric gauge choices are discussed and necessary for formulating energy invariant biorthogonal electronic equations. Our method is further applied to characterize vibrationally averaged molecular bonding properties of molecular energetics, bond length, protonic and electron density. Moreover, post-Hartree-Fock electron correlation can be conveniently computed on the basis of nucleus-electron coupled molecular orbitals, as demonstrated to correlated models of second-order Møller-Plesset perturbation and full configuration interaction theories. Our approach not only accurately quantifies non-classical nucleus-electron couplings for revising molecular bonding properties, but also provides an alternative time-independent approach for deploying non-BO molecular quantum chemistry.

^{a)}Electronic mail: juny@hku.hk

I. INTRODUCTION

The Born-Oppenheimer (BO) approximation¹ is the fundamental cornerstone of modern electronic structure theories, providing computational framework in which a broad range of chemical properties can be conveniently computed. For instances, the BO approximation leads to the adiabatic electronic potential energy surface (PES) with respect to nuclear positions, molecular geometric structures obtained at PES stationary locations that are often compared to experimentally resolved bond lengths and angles, the reaction kinetics and pathways on a single PES where bonds are broken and made, infrared spectroscopy from bond vibrations, and many others. However, since the BO approximation accounts for only classical couplings for nucleus-electron pairs, it breaks down when the non-classical nucleus-electron correlation contributes significantly to such chemical processes involving light proton as proton-coupled electron transfer,²⁻⁶ nonadiabatic quantum nuclear tunneling between close PESs,⁷⁻⁹ and so on. The presence of strongly correlated nucleus-electron motion may fundamentally alter the density distributions of non-classical nuclei and electrons, giving rise to different bonding characters and chemical connections averaged on nuclear trajectories.

Many theoretical methods have been developed to address non-BO effects.¹⁰⁻¹² The most straightforward non-BO scheme is the diagonal BO correction (DBOC) from the second derivative coupling between adiabatic wavefunctions.^{13,14} The multi-configurational time-dependent Hartree (MCTDH)^{15,16} method determines the motion of quantal nuclei on several coupled PESs by superposing the product states of electronic and nuclear wavefunctions. The explicit correlated Gaussian (ECG) based non-BO theory, uses the conventional Cartesian coordinates and ECG basis functions to build many-body molecular wavefunction, which has been shown to converge nucleus-electron correlation rapidly with the expansion length.¹⁷ Quantum Monte Carlo (QMC) such as fixed-node diffusion QMC (FN-DMC)^{18,19} has been demonstrated to include a nuclear wavefunction as the products of Gaussian functions on nuclear pairs. These methods have been demonstrated to be able to achieve high accuracy, but are also challenged by large computational costs that limit their application to non-BO effect of small systems.²⁰

Moreover, significant efforts in developing non-BO formalism have been devoted to the orbital representation of nuclei, originating from the idea of the protonic wavefunctions using one-proton Slater-type functions centered on heavier nuclei by Thomas.²¹⁻²³ This drove the introduction of more general Gaussian-type nuclear orbitals (NOs) on an equal footing to electronic molecular or-

bitals (MOs), and led to the development of various multicomponent-MO methods in which both electronic and nuclear wavefunctions are computed simultaneously to incorporate nucleus-electron correlation and nuclear quantum effects, as implemented at both mean-field and correlated quantum chemical levels of theory including many-body perturbation theory, coupled-cluster and configuration interaction models.^{24–29} The multicomponent MO provides a framework which is exact to non-BO problems if it would be possible to perform the full configuration interaction (FCI) expansion on the mean-field references for both electrons and nuclei.³⁰ Most recently, the multicomponent nuclear-electronic orbital³¹ (NEO) method has revitalized the idea of nuclear orbital to represent both classical and quantized nuclei: a number of modern quantum chemistry variants from NEO Hamiltonian and explicitly correlated wavefunction have been developed and applied to non-BO studies,^{32–34} for methods including density functional theory (NEO-DFT),^{35,36} constrained NEO-DFT (cNEO-DFT)^{37–39} and time-dependent DFT (NEO-TDDFT),^{40,41} coupled-cluster singles and doubles (NEO-CCSD),⁴² orbital-optimized second-order Møller-Plesset (MP2) perturbation (NEO-OOMP2) and coupled-cluster with doubles (NEO-OOCCD),³⁴ and the complete-active space SCF (NEO-CASSCF).⁴³ As the NEO Hamiltonian is nuclei-clamped for classical nuclei by assuming fixed nuclear coordinates, the difficulties with rotational and translational degrees of freedom are avoided.³¹ Beyond multicomponent HF that neglects electron-proton correlation, Brorsen suggested that accurate protonic densities can be obtained from a truncated heat-bath CI expansion (HCI-NEO-CISDTQ)⁴⁴ only if excitations up to quadruples are included, or the poor multicomponent HF orbitals are optimized in the presence of electron-proton correlation.^{45,46}

In principle, a rigorous separation of electronic and nuclear motion can be represented in the Born-Huang (BH) expansion of the total molecular wavefunction using complete adiabatic eigenstates of BO Hamiltonian. Alternative to BH, an exact probability decomposition was attempted by Hunter in the early days⁴⁷: the full molecular wavefunction $\Psi(\mathbf{rs}, \mathbf{R})$ was factorized into a single product of a non-BO electronic wavefunction (as the conditional probability amplitude $\Phi(\mathbf{rs}, \mathbf{R})$ for electrons at \mathbf{rs} in the presence of all nuclei) and a nuclear wavefunction (as the marginal probability amplitude $\chi(\mathbf{R})$ for nuclei at \mathbf{R}),

$$\Psi(\mathbf{rs}, \mathbf{R}) = \Phi(\mathbf{rs}, \mathbf{R})\chi(\mathbf{R}). \quad (1)$$

Recently, Gross et al. has shown that given partial normalization condition, such an exact factorization exists and is unique for defining electronic and nuclear subsystems, up to a phase factor. The exactly factorized wavefunction has been investigated and validated for both time-

independent^{48–52} and time-dependent^{53,54} non-BO simulations of several model systems for which the original full problem is solved and the factorization of Eq. (1) is then inverted to obtain electronic and nuclear subsystem wavefunctions.^{55–57} A self-consistent numerical approach for the time-dependent solution of coupled electron-ion dynamics has been demonstrated to Shin-Metiu model system recently.⁵⁸

Based on Hunter’s wavefunction probability interpretation for including non-BO impacts, we propose a time-independent SCF method in which the mean-field molecular wavefunction for quantum chemistry Hamiltonian is factorized into a unique single product associated with non-BO electronic MOs and the numerically exact vibrational wavefunction of nuclei. In this work, we develop a computationally systematic and convenient approach of self-consistently capturing non-classical nucleus-electron couplings for uncorrelated electrons, and use resulting non-BO MOs and exact nucleus-electron embedding potential to further build up electronic correlations in the well established context of *ab-initio* molecular quantum chemistry. By computing and assessing non-BO effects on energies, chemical bond lengths, electron and nuclear density distributions, we will demonstrate that our method can accurately quantify nucleus-electron correlations which address vibrationally averaged bonding patterns, from a mean-field single product wavefunction.

II. THEORY

We adopt the following notation in our formulation. The occupied, virtual and general MOs are labeled by $\{i, j, k, \dots\}$, $\{a, b, c, \dots\}$ and $\{p, q, r, \dots\}$, respectively. The MOs and their biorthogonal counterparts are respectively denoted as ψ_p and $\bar{\psi}_p$. The molecular geometry is collectively signified by \mathbf{R} , and \mathbf{r} and \mathbf{s} represent the spatial and spin coordinates of electrons, respectively. Generically, \hat{O} and \mathbf{O} are used to denote an operator and the corresponding matrix form, respectively, with the latter composed of the matrix elements by O_{pq} .

A. Molecular wavefunction factorization

Consider an H^- anion that constitutes a minimum correlated non-BO atom. Apparently, the three-body correlation emerges between the electron pair and the proton, which complicates non-BO treatments within the hierarchy of correlated quantum chemistry. Nonetheless, the original complex three-body problem can be approximately cast into additive two-body problems in which

the electron-electron and electron-proton correlations can be separately computed when a single PES dominates. To this end, we begin with defining the full one-electron nucleus-electron wavefunction $\tilde{\psi}_i(\mathbf{r}_j\mathbf{s}_j, \mathbf{R})$ in an exact factorization as follows,

$$\tilde{\psi}_i(\mathbf{r}_j\mathbf{s}_j, \mathbf{R}) = \psi_i(\mathbf{r}_j\mathbf{s}_j, \mathbf{R})\chi(\mathbf{R}) \quad (2)$$

which is analogous to that of the full many-electron molecular wavefunction of Eq. (1). $\psi_i(\mathbf{r}_j\mathbf{s}_j, \mathbf{R})$, which we term a non-BO electronic MO, resembles the conditional probability amplitude of finding an electron in a mean-field potential dressed in nucleus-electron correlation that explicitly depends on nuclear coordinates. The mean-field molecular wavefunction can be built by making a single product Eq. (1) between the non-BO electronic determinant $\Phi(\mathbf{rs}, \mathbf{R})$ and nuclear wavefunctions $\chi(\mathbf{R})$,

$$\Phi(\mathbf{rs}, \mathbf{R}) = |\psi_1(\mathbf{r}_1\mathbf{s}_1, \mathbf{R}), \psi_2(\mathbf{r}_2\mathbf{s}_2, \mathbf{R}), \dots, \psi_{N_e}(\mathbf{r}_{N_e}\mathbf{s}_{N_e}, \mathbf{R})\rangle, \quad (3)$$

for a free molecule of N_e electrons. This requires a normalization for $\Psi(\mathbf{rs}, \mathbf{R})$ on both electronic and nuclear coordinates,

$$\int d\mathbf{R} \langle \Psi(\mathbf{rs}, \mathbf{R}) | \Psi(\mathbf{rs}, \mathbf{R}) \rangle_{\mathbf{rs}} = 1 \quad (4)$$

and a partial normalization condition (PNC) for the determinant and thus non-BO MOs at any molecular geometry \mathbf{R}

$$\langle \psi_i(\mathbf{rs}, \mathbf{R}) | \psi_i(\mathbf{rs}, \mathbf{R}) \rangle_{\mathbf{rs}} = 1 \quad (5)$$

where $\langle | \rangle_{\mathbf{rs}}$ indicates the normalization on the electronic coordinates only. This makes the unique decomposition of Eqs. (2) and (1), up to only a gauge transformation. The coupled product of Eq. (1) is to be distinguished from the BO factorization $\Psi(\mathbf{rs}, \mathbf{R}) \approx \Phi^{\text{BO}}(\mathbf{rs}, \mathbf{R})\chi^{\text{BO}}(\mathbf{R})$ in which $\Phi^{\text{BO}}(\mathbf{rs}, \mathbf{R})$ must be a solution to the BO electronic equation that parametrically depends on a geometry \mathbf{R} . However, the BO product does not account for nucleus-electron correlation, which can be recovered via the coupled product that encodes the mutual dependence between electrons and nuclei. A tensor-product framework for constructing the total wavefunction in molecular Hilbert space has been also demonstrated recently.⁵⁹

B. Exact nucleus-electron potential embedding uncorrelated electrons

In our approach, the full correlation between the nuclear and electronic subsystems is determined via an SCF procedure in which the mutual response to the electronic and nuclear impact

from each other must be variationally recovered by minimizing the total molecular energy functional \mathcal{L} in terms of $\Phi(\mathbf{r}\mathbf{s}, \mathbf{R})$ and $\chi(\mathbf{R})$, subject to the normalization conditions in the electronic and nuclear coordinate space, respectively.

$$\begin{aligned} \mathcal{L} = & \int d\mathbf{R} \langle \Psi(\mathbf{r}\mathbf{s}, \mathbf{R}) | \hat{H} | \Psi(\mathbf{r}\mathbf{s}, \mathbf{R}) \rangle_{\mathbf{r}\mathbf{s}} - \int d\mathbf{R} E_{el}(\mathbf{R}) [\langle \Phi(\mathbf{r}\mathbf{s}, \mathbf{R}) | \Phi(\mathbf{r}\mathbf{s}, \mathbf{R}) \rangle_{\mathbf{r}\mathbf{s}} - 1] \\ & - E [\langle \chi(\mathbf{R}) | \chi(\mathbf{R}) \rangle_{\mathbf{R}} - 1] \end{aligned} \quad (6)$$

with the multipliers $E_{el}(\mathbf{R})$ and E to enforce the PNC and nuclear normalization conditions, respectively. The full molecular Hamiltonian \hat{H} is

$$\hat{H} = \hat{H}_{\text{BO}} + \hat{T}_n. \quad (7)$$

where \hat{H}_{BO} is the regular BO Hamiltonian. \hat{T}_n is the nuclear kinetic operator for all internal nuclear motions, i.e., the atomic vibrations are separated from the continuum states associated with the center of mass translation and the whole rotation of a free molecule, with the latter providing only a constant energy shift. The spatial part of non-BO MO $\psi_i(\mathbf{r}, \mathbf{R})$ is expanded in atomic orbitals (AO) $\phi_\alpha(\mathbf{r}, \mathbf{R})$ through molecular coefficients $C_{\alpha i}$ as an explicit function of nuclear positions.

$$\psi_i(\mathbf{r}, \mathbf{R}) = \sum_{\alpha} C_{\alpha i}(\mathbf{R}) \phi_{\alpha}(\mathbf{r}, \mathbf{R}). \quad (8)$$

For a single determinant wavefunction in Eq. (3), the Lagrangian energy of Eq. (6) can be cast into the form (see Eq. (A1) in Appendix A) in terms of biorthogonal non-BO MOs $\psi_i(\mathbf{r}, \mathbf{R})$, and variationally minimized with respect to $C_{\alpha i}(\mathbf{R})$, $\chi(\mathbf{R})$, the multipliers $\tilde{\epsilon}_{ij}(\mathbf{R})$ and the total energy E . The derivation is presented in Appendix A and yields the non-BO coupled electronic and nuclear equations in terms of a nucleus-electron correlation potential for electrons and an electronic energy potential for nuclei as follows, respectively,

$$\left(\hat{F}_{\text{BO}} + \hat{V}_{\chi}^{\text{cp}} + \frac{\chi^{\dagger}(\mathbf{R}) \hat{T}_n \chi(\mathbf{R})}{|\chi(\mathbf{R})|^2} \right) |\psi_i\rangle = \frac{\epsilon_i(\mathbf{R})}{|\chi(\mathbf{R})|^2} |\psi_i\rangle, \quad (9)$$

$$(\hat{T}_n + E_{el}(\mathbf{R})) \chi = E \chi. \quad (10)$$

\hat{F}_{BO} is the BO Fock operator. The vibrational kinetic energy $\chi^{\dagger}(\mathbf{R}) \hat{T}_n \chi(\mathbf{R}) / |\chi(\mathbf{R})|^2$ provides constant shift to $\epsilon_i(\mathbf{R})$ for each geometry and can be excluded from Eq. (9). The value of the multiplier E is the exact total molecular energy, and the electronic $E_{el}(\mathbf{R}) = \langle \Phi(\mathbf{r}, \mathbf{R}) | \hat{H} | \Phi(\mathbf{r}, \mathbf{R}) \rangle_{\mathbf{r}} - \sum_{\nu} \frac{1}{M_{\nu}} \langle \Phi(\mathbf{r}, \mathbf{R}) | \nabla_{\nu} | \Phi(\mathbf{r}, \mathbf{R}) \rangle_{\mathbf{r}} \cdot \nabla_{\nu}$ defines the non-BO PES on which nuclei move, but also depends on nuclear wavefunction. $\hat{V}_{\chi}^{\text{cp}}$ is the nonlinear nucleus-electron embedding operator that

depends on the embedded one-electron states $|\psi_i\rangle$ and $\langle\bar{\psi}_j|$, their nuclear derivatives and the nuclear wavefunction χ ,

$$\hat{V}_\chi^{\text{cp}} = -\sum_{\mathbf{v}} \frac{1}{M_{\mathbf{v}}} \left(\frac{\nabla_{\mathbf{v}}\chi}{\chi} \cdot \nabla_{\mathbf{v}} + \frac{\nabla_{\mathbf{v}}^2}{2} + \sum_j \langle\bar{\psi}_j|\nabla_{\mathbf{v}}\psi_j\rangle \cdot \nabla_{\mathbf{v}} - |\nabla_{\mathbf{v}}\psi_j\rangle \cdot \langle\bar{\psi}_j|\nabla_{\mathbf{v}} \right). \quad (11)$$

Here, the first term $\frac{\nabla_{\mathbf{v}}\chi}{\chi} \cdot \nabla_{\mathbf{v}}$ is important to capture the derivative coupling with nuclear motion, proportional to the first geometric gradients of both electronic and nuclear wavefunctions. The remaining three terms account for $\langle\Phi(\mathbf{r}, \mathbf{R})|\hat{T}_n|\Phi(\mathbf{r}, \mathbf{R})\rangle_{\mathbf{r}}$ which formally confirms the SCF DBOC contribution,⁶⁰ but in terms of $\Phi(\mathbf{r}, \mathbf{R})$ that is self-consistently coupled to the nuclear motion via \hat{V}_χ^{cp} . \hat{V}_χ^{cp} represents the exact correlation potential with nuclei over their internal coordinates \mathbf{v} (e.g., vibrational modes) for embedding uncorrelated electrons non-classically, which must necessitate a self-consistent procedure to solve Eqs. (9) for $\psi_i(\mathbf{r}, \mathbf{R})$ and (10) for $\chi(\mathbf{R})$. Our approach is therefore termed nucleus-electron coupled self-consistent field (NECSCF) method which must converge both the PES $E_{el}(\mathbf{R})$ and the total molecular energy E . Eqs. (9) and (11) are solved for MOs to build a Slater determinant, and the generalization to multiconfigurational electronic wavefunction is feasible by adopting a linear combination of configurations in Eq. (1). The resulting MOs $\psi_i(\mathbf{r}, \mathbf{R})$ naturally lead to post-Hartree-Fock treatment of correlated electrons in the presence of the exact quantum embedding potential $\hat{V}^{\text{cp}}(\chi)$ from nuclear subsystems that are governed on a single PES. We thus further implemented the NECSCF-based second-order Møller-Plesset perturbation (NECSCF-MP2) theory and the full configuration interaction (NECSCF-FCI).

The nucleus-electron embedding potential $\hat{V}^{\text{cp}}(\chi)$ must be solved in the presence of the derivative operator $\nabla_{\mathbf{v}} = \frac{\partial}{\partial \mathbf{R}_{\mathbf{v}}}$ in Eq. (11) for including the non-BO relaxation of an electron that correlates with nuclei. As $\hat{F} = \hat{F}_{BO} + \hat{V}_\chi^{\text{cp}}$ is not self-adjoint due to $\frac{\nabla_{\mathbf{v}}\chi}{\chi} \cdot \nabla_{\mathbf{v}}$, the following biorthogonal equation is solved for non-Hermitian system⁶¹ for its conjugate Hamiltonian,

$$\hat{F}^\dagger |\bar{\psi}_i\rangle = \frac{\bar{\epsilon}_i(\mathbf{R})}{|\chi|^2} |\bar{\psi}_i\rangle. \quad (12)$$

with the biorthogonality $\langle\bar{\psi}_i|\psi_j\rangle = \langle\psi_i|\bar{\psi}_j\rangle = \delta_{ij}$ and $\bar{\epsilon}_i^*(\mathbf{R}) = \epsilon_i(\mathbf{R})$.

C. Geometric gauge choice making energy invariant

For general biorthogonal non-BO MOs that lose complex conjugation, the first-derivative $\langle\bar{\psi}_i|\nabla_{\mathbf{v}}\psi_j\rangle$ may be no longer anti-symmetric which may break the invariance of electronic energy upon an unitary rotation within the respective internal space on $|\psi_i\rangle$ and $|\bar{\psi}_i\rangle$. The elements

of the geometric derivative vectors $\mathbf{A}^{(v)}$ and $\bar{\mathbf{A}}^{(v)}$ are

$$A_{pq}^{(v)} = \langle \bar{\psi}_p | \nabla_v \psi_q \rangle \quad (13)$$

$$\bar{A}_{pq}^{(v)} = \langle \psi_p | \nabla_v \bar{\psi}_q \rangle, \quad (14)$$

Based on the derivative biorthogonality from

$$\nabla_v \langle \bar{\psi}_p | \psi_q \rangle = 0, \quad (15)$$

\mathbf{A} and $\bar{\mathbf{A}}$ must be related to each other as,

$$\bar{\mathbf{A}}^{\dagger(v)} = -\mathbf{A}^{(v)}. \quad (16)$$

Many geometric gauges that fulfill the biorthogonality condition of Eq. (15) can be envisioned. In the present work, we construct a set of legitimate $U_{ij}^{(v)}$ and $\bar{U}_{ij}^{(v)}$ that are composed of symmetric and anti-symmetric components among the occupied MOs,

$$U_{ij}^{(v)} = -\frac{1}{2} (\bar{\mathbf{C}}_i^\dagger \mathbf{S}^{0v} \mathbf{C}_j + \bar{\mathbf{C}}_j^\dagger \mathbf{S}^{0v} \mathbf{C}_i) - \frac{1}{2} (\bar{\mathbf{C}}_i^\dagger \mathbf{S}^{v0} \mathbf{C}_j - \bar{\mathbf{C}}_j^\dagger \mathbf{S}^{v0} \mathbf{C}_i), \quad (17)$$

$$\bar{U}_{ij}^{(v)} = -\frac{1}{2} (\mathbf{C}_i^\dagger \mathbf{S}^{0v} \bar{\mathbf{C}}_j + \mathbf{C}_j^\dagger \mathbf{S}^{0v} \bar{\mathbf{C}}_i) - \frac{1}{2} (\mathbf{C}_i^\dagger \mathbf{S}^{v0} \bar{\mathbf{C}}_j - \mathbf{C}_j^\dagger \mathbf{S}^{v0} \bar{\mathbf{C}}_i). \quad (18)$$

Above, the derivative overlaps are $S_{\alpha\beta}^{0v} = \langle \phi_\alpha | \nabla_v \phi_\beta \rangle$ and $S_{\alpha\beta}^{v0} = \langle \nabla_v \phi_\alpha | \phi_\beta \rangle$. Similar constructions can be drawn to virtual MOs. This gives rise to the anti-symmetric $A_{ij}^{(v)}$ and $\bar{A}_{ij}^{(v)}$,

$$A_{ij}^{(v)} = -\frac{1}{2} (\bar{\mathbf{C}}_j^\dagger \mathbf{S}^{0v} \mathbf{C}_i - \bar{\mathbf{C}}_i^\dagger \mathbf{S}^{0v} \mathbf{C}_j) - \frac{1}{2} (\bar{\mathbf{C}}_i^\dagger \mathbf{S}^{v0} \mathbf{C}_j - \bar{\mathbf{C}}_j^\dagger \mathbf{S}^{v0} \mathbf{C}_i), \quad (19)$$

$$\bar{A}_{ij}^{(v)} = -\frac{1}{2} (\mathbf{C}_j^\dagger \mathbf{S}^{0v} \bar{\mathbf{C}}_i - \mathbf{C}_i^\dagger \mathbf{S}^{0v} \bar{\mathbf{C}}_j) - \frac{1}{2} (\mathbf{C}_i^\dagger \mathbf{S}^{v0} \bar{\mathbf{C}}_j - \mathbf{C}_j^\dagger \mathbf{S}^{v0} \bar{\mathbf{C}}_i) \quad (20)$$

Obviously the diagonal elements must be zero

$$A_{ii}^{(v)} = \bar{A}_{ii}^{(v)} = 0. \quad (21)$$

As we will further show in Appendix C, any unitary rotation among all occupied MOs adds merely a phase factor to the total molecular wavefunction $\Psi(\mathbf{r}\mathbf{s}, \mathbf{R})$, leaving both electronic and molecular energies invariant. This is essential to orbital localization and diabaticization techniques based on NECSCF MOs as derived from the electronic equation.

Moreover, another gauge transformation is possible by combining the Hermitian and anti-Hermitian terms as follows

$$U_{ij}^{(v)} = -\frac{1}{2} (\bar{\mathbf{C}}_i^\dagger \mathbf{S}^{0v} \mathbf{C}_j + \mathbf{C}_i^\dagger \mathbf{S}^{v0} \bar{\mathbf{C}}_j) - \frac{1}{2} (\bar{\mathbf{C}}_i^\dagger \mathbf{S}^{v0} \mathbf{C}_j - \mathbf{C}_i^\dagger \mathbf{S}^{0v} \bar{\mathbf{C}}_j), \quad (22)$$

$$\bar{U}_{ij}^{(v)} = -\frac{1}{2} (\bar{\mathbf{C}}_i^\dagger \mathbf{S}^{v0} \mathbf{C}_j + \mathbf{C}_i^\dagger \mathbf{S}^{0v} \bar{\mathbf{C}}_j) - \frac{1}{2} (\mathbf{C}_i^\dagger \mathbf{S}^{v0} \bar{\mathbf{C}}_j - \bar{\mathbf{C}}_i^\dagger \mathbf{S}^{0v} \mathbf{C}_j), \quad (23)$$

giving the following anti-Hermitian derivative vectors ,

$$A_{ij}^{(v)} = \bar{A}_{ij}^{(v)} = -\frac{1}{2} \left(\bar{\mathbf{C}}_i^\dagger \mathbf{S}^{v0} \mathbf{C}_j - \mathbf{C}_i^\dagger \mathbf{S}^{0v} \bar{\mathbf{C}}_j \right) - \frac{1}{2} \left(\mathbf{C}_i^\dagger \mathbf{S}^{v0} \bar{\mathbf{C}}_j - \bar{\mathbf{C}}_i^\dagger \mathbf{S}^{0v} \mathbf{C}_j \right). \quad (24)$$

A stronger condition can be therefore examined by enforcing all derivative elements $A_{ij}^{(v)} = 0$,

$$\bar{\mathbf{C}}_i^\dagger (\mathbf{S}^{v0} - \mathbf{S}^{0v}) \mathbf{C}_j = -\mathbf{C}_i^\dagger (\mathbf{S}^{v0} - \mathbf{S}^{0v}) \bar{\mathbf{C}}_j. \quad (25)$$

Apparently, the condition in Eq. (25) is Hermitian and leads to energy invariant formulation, but may be difficult to occur simultaneously for general many-electron molecules. Detailed numerical studies on its possibility to the localization/diabatization of NECSCF MOs will be exploited in our future work.

D. Working equation and approximation

Under the transformations in Eqs. (17) and (18), the embedding operator \hat{V}_χ^{cp} can be reduced to

$$\hat{V}_\chi^{\text{cp}} = -\sum_{\mathbf{v}} \frac{1}{M_{\mathbf{v}}} \left(\frac{\nabla_{\mathbf{v}} \chi}{\chi} \cdot \nabla_{\mathbf{v}} + \frac{\nabla_{\mathbf{v}}^2}{2} - \sum_j |\nabla_{\mathbf{v}} \psi_j\rangle \cdot \langle \bar{\psi}_j | \nabla_{\mathbf{v}} \right) \quad (26)$$

with the last two terms accounting for the contribution from nuclear kinetic operator. As shown in Appendix A, \hat{V}_χ^{cp} is form-invariant upon an unitary rotation among occupied MOs. By employing the identity operator $\mathbf{I} = \sum_p |\psi_p\rangle \langle \bar{\psi}_p |$ in the full spectrum of non-BO MOs,

$$\begin{aligned} \nabla_{\mathbf{v}}^2 |\psi_i\rangle &= \nabla_{\mathbf{v}} \cdot \left(\sum_p |\psi_p\rangle \langle \bar{\psi}_p | \nabla_{\mathbf{v}} \psi_i \right) \\ &= \sum_p |\nabla_{\mathbf{v}} \psi_p\rangle \cdot \langle \bar{\psi}_p | \nabla_{\mathbf{v}} \psi_i \rangle + \sum_p |\psi_p\rangle \nabla_{\mathbf{v}} \cdot \langle \bar{\psi}_p | \nabla_{\mathbf{v}} \psi_i \rangle \end{aligned} \quad (27)$$

there is

$$\begin{aligned} & \frac{\nabla_{\mathbf{v}}^2}{2} - \sum_j |\nabla_{\mathbf{v}} \psi_j\rangle \cdot \langle \bar{\psi}_j | \nabla_{\mathbf{v}} \\ &= \nabla_{\mathbf{v}}^2 - \sum_j |\nabla_{\mathbf{v}} \psi_j\rangle \cdot \langle \bar{\psi}_j | \nabla_{\mathbf{v}} - \frac{\nabla_{\mathbf{v}}^2}{2} \\ &= \left(\sum_p |\nabla_{\mathbf{v}} \psi_p\rangle \cdot \langle \bar{\psi}_p | \nabla_{\mathbf{v}} + \sum_p |\psi_p\rangle \nabla_{\mathbf{v}} \cdot \langle \bar{\psi}_p | \nabla_{\mathbf{v}} \right) - \sum_j |\nabla_{\mathbf{v}} \psi_j\rangle \cdot \langle \bar{\psi}_j | \nabla_{\mathbf{v}} - \frac{\nabla_{\mathbf{v}}^2}{2} \\ &= \sum_a |\nabla_{\mathbf{v}} \psi_a\rangle \cdot \langle \bar{\psi}_a | \nabla_{\mathbf{v}} + \sum_p |\psi_p\rangle \nabla_{\mathbf{v}} \cdot \langle \bar{\psi}_p | \nabla_{\mathbf{v}} - \frac{\nabla_{\mathbf{v}}^2}{2}. \end{aligned} \quad (28)$$

The integration of Eq. (28) between $\bar{\psi}_i$ and ψ_j over their electronic coordinates yields the following element, which is termed $Y_{ij}^{(v)}$,

$$\begin{aligned}
Y_{ij}^{(v)} &= \sum_a A_{ia}^{(v)} \cdot A_{aj}^{(v)} + \nabla_v \cdot A_{ij}^{(v)} - \left\langle \bar{\psi}_i \left| \frac{\nabla_v^2}{2} \psi_j \right. \right\rangle \\
&= \sum_a A_{ia}^{(v)} \cdot A_{aj}^{(v)} + \nabla_v \cdot A_{ij}^{(v)} - \frac{1}{2} (\nabla_v \cdot \langle \bar{\psi}_i | \nabla_v \psi_j \rangle - \langle \nabla_v \bar{\psi}_i | \nabla_v \psi_j \rangle) \\
&= \sum_a A_{ia}^{(v)} \cdot A_{aj}^{(v)} + \frac{1}{2} \nabla_v \cdot A_{ij}^{(v)} + \frac{1}{2} \langle \nabla_v \bar{\psi}_i | \nabla_v \psi_j \rangle
\end{aligned} \tag{29}$$

Here the first term is quite small and thus neglected in our solver of electronic equation, as the product $A_{ia}A_{aj}$ is inversely proportional to the product of the difference between occupied and virtual orbital energies $\frac{1}{(\epsilon_a - \epsilon_i)(\epsilon_j - \epsilon_a)}$. A linearization of the second term is made by using the first-order Taylor expansion of the derivative $A_{ij}^{(v)}$ with respect to the vibrational coordinates,

$$\nabla_v \cdot A_{ij}^{(v)} \approx \nabla_v \cdot [A_{ij}^{(v)}]_{\mathbf{R}_0} + \nabla_v \cdot \sum_{v'} v' [\nabla_{v'} \cdot A_{ij}^{(v)}]_{\mathbf{R}_0} = [\nabla_v \cdot A_{ij}^{(v)}]_{\mathbf{R}_0} \tag{30}$$

which indicates that the divergence of the NECSCF first-derivative vector can be approximated by that at the unperturbed geometry where the BO approximation is assumed. Since $\nabla_v \cdot A_{ij}^{(v)}$ makes no direct contribution to the electronic energy due to the diagonal $A_{ii}^{(v)} = 0$ and the off-diagonal contribution from the BO-based $[A_{ij}^{(v)}]_{\mathbf{R}_0}$ to the embedding operator is real, and usually very small compared to $\frac{\nabla_v \chi}{\chi} \cdot A_{ij}^{(v)}$, the divergence term $\nabla_v \cdot A_{ij}^{(v)}$ is not important and thus neglected as well in solving NECSCF electronic states. The last contribution $\langle \nabla_v \bar{\psi}_i | \nabla_v \psi_j \rangle$ is also usually neglected. Finally, only $\frac{\nabla_v \chi}{\chi} \cdot \nabla_v$ operator is practically important and implemented in the AO basis for solving NECSCF one-electron states. The $Y_{ij}^{(v)}$ contributions that are not included for SCF solution can be simply patched to NECSCF orbital energies using the converged NECSCF MOs.

$$\mathbf{V}_\chi^{\text{cp}} = - \sum_v \frac{1}{M_v} \frac{\nabla_v \chi(\mathbf{R})}{\chi(\mathbf{R})} [\mathbf{S}(\nabla_v \mathbf{C}) \bar{\mathbf{C}}^\dagger \mathbf{S} + \mathbf{S}^{0v}], \tag{31}$$

$$\mathbf{V}_\chi^{\dagger \text{cp}} = \sum_v \frac{1}{M_v} \frac{\nabla_v \chi^\dagger(\mathbf{R})}{\chi^\dagger(\mathbf{R})} [\mathbf{S}(\nabla_v \bar{\mathbf{C}}) \mathbf{C}^\dagger \mathbf{S} + \mathbf{S}^{0v}] \tag{32}$$

The coupled perturbed Hartree-Fock (CPHF) is formulated for biorthogonal NECSCF system to compute $\nabla_v \mathbf{C}$ and $\nabla_v \bar{\mathbf{C}}$, based on the first-order geometric relaxation $\mathbf{U}^{(v)}$ and $\bar{\mathbf{U}}^{(v)}$ of one-electron state embedded in the non-Hermitian nucleus-electron potential. $\mathbf{U}^{(v)}$ and $\bar{\mathbf{U}}^{(v)}$ are related

through the derivative biorthogonality between the eigenstates of \hat{F} and \hat{F}^\dagger ,

$$\mathbf{U}^{(v)} + \bar{\mathbf{U}}^{\dagger(v)} + \mathcal{S}^{(v)} = 0, \quad (33)$$

where in the MO basis

$$\mathcal{S}^{(v)} = \bar{\mathbf{C}}^\dagger (\mathbf{S}^{0v} + \mathbf{S}^{v0}) \mathbf{C}. \quad (34)$$

Apparently, as $\bar{\mathbf{U}}^{\dagger(v)}$ is not assumed to be conjugated with $\mathbf{U}^{(v)}$ which normally holds in BO methods, both the occupied-virtual relaxation ($U_{ia}^{(v)}$) and virtual-occupied relaxation ($U_{ai}^{(v)}$) must be explicitly solved from the CPHF equations,

$$\begin{aligned} [\varepsilon_q - \varepsilon_p] U_{pq}^{(v)} = & \sum_k^{\text{occ}} \langle pk || qk \rangle^{(v)} + \mathcal{H}_{pq}^{(v)} - \mathcal{S}_{pq}^{(v)} \varepsilon_q - \sum_{jk}^{\text{occ}} \mathcal{S}_{kj}^{(v)} \langle pj || qk \rangle \\ & + \sum_k^{\text{occ}} \sum_b^{\text{vir}} \left[U_{bk}^{(v)} \langle pk || qb \rangle - U_{kb}^{(v)} \langle pb || qk \rangle - \mathcal{S}_{kb}^{(v)} \langle pb || qk \rangle \right] \end{aligned} \quad (35)$$

where the one-electron derivative core Hamiltonian is $\mathcal{H}_{pq}^{(v)} = \bar{\mathbf{C}}_p^\dagger \mathbf{G}_{\text{NECSFC}}^{(v)} \mathbf{C}_q$. Once $U_{ia}^{(v)}$ and $U_{ai}^{(v)}$ are solved, the relaxations $\bar{U}_{ia}^{(v)}$ and $\bar{U}_{ai}^{(v)}$ are thus computed using Eq. (33).

It should be pointed out that the derivative core Hamiltonian $\mathbf{G}_{\text{NECSFC}}^{(v)}$ contains the NECSFC contribution from the nucleus-electron embedding potential. According to the first-order response of $\frac{\nabla_v \chi(\mathbf{R})}{\chi(\mathbf{R})} \cdot \nabla_v$ operator in AO matrix form,

$$\nabla_v \sum_{v'} \frac{1}{M_{v'}} \frac{\nabla_{v'} \chi(\mathbf{R})}{\chi(\mathbf{R})} \cdot \mathbf{A}^{(v')} = \sum_{v'} \frac{1}{M_{v'}} \nabla_v \left[\frac{\nabla_{v'} \chi(\mathbf{R})}{\chi(\mathbf{R})} \right] \cdot \mathbf{A}^{(v')} + \sum_{v'} \frac{1}{M_{v'}} \frac{\nabla_{v'} \chi(\mathbf{R})}{\chi(\mathbf{R})} \cdot \nabla_v \mathbf{A}^{(v')} \quad (36)$$

Using similar analysis according to Eq. (30), $\nabla_v \mathbf{A}^{(v')} \approx \left[\nabla_v \mathbf{A}^{(v')} \right]_{\mathbf{R}_0}$ is unimportant and neglected to avoid second geometric derivative. Further assuming the vibrational product state for independent vibrational wavefunctions $\chi_v(\mathbf{R})$, there is

$$\frac{\nabla_v \chi(\mathbf{R})}{\chi(\mathbf{R})} = \frac{\nabla_v \chi_v(\mathbf{R})}{\chi_v(\mathbf{R})}, \quad (37)$$

and therefore

$$\nabla_v \left[\frac{\nabla_{v'} \chi(\mathbf{R})}{\chi(\mathbf{R})} \right] = \delta_{vv'} \nabla_v \left[\frac{\nabla_{v'} \chi_{v'}(\mathbf{R})}{\chi_{v'}(\mathbf{R})} \right]. \quad (38)$$

We then admit the following working form of $\mathbf{G}_{\text{NECSFC}}^{(v)}$,

$$\mathbf{G}_{\text{NECSFC}}^{(v)} = \mathbf{G}_{\text{BO}}^{(v)} - \sum_v \frac{1}{M_v} \nabla_v \left[\frac{\nabla_v \chi_v(\mathbf{R})}{\chi_v(\mathbf{R})} \right] \cdot \mathbf{A}^{(v)} \quad (39)$$

with $\mathbf{G}_{\text{BO}}^{(v)}$ the derivative of the regular core Hamiltonian accounting for the electronic kinetic and classical nucleus-electron attraction energies computed in the BO framework. Analytical first- and second-derivatives $\nabla_v \chi_v$ and $\nabla_v^2 \chi_v$ of vibrational wavefunction χ_v are implemented (Appendix D).

Two simple scenarios can be analyzed based on Eqs. (31), (32) and (39) to exam the significance of correlated nucleus-electron behaviour. Around equilibrium structure, the ground vibrational wavefunction χ_v can be approximated as Gaussian function for which $\frac{\nabla_v \chi_v(\mathbf{R})}{\chi_v(\mathbf{R})}$ is proportional to vibrational displacement and $\nabla_v \left[\frac{\nabla_v \chi_v(\mathbf{R})}{\chi_v(\mathbf{R})} \right]$ proportional to frequency ω_v of this mode, i.e., higher-frequency modes and moderately stretched bonds tend to strengthen nucleus-electron correlation. However, at the dissociation region where the electronic potential becomes flat, the ground vibrational wavefunction carries the landscape asymptotically approaching an exponential function for which the NECSCF contribution is eventually zero due to $\nabla_v \left[\frac{\nabla_v \chi_v(\mathbf{R})}{\chi_v(\mathbf{R})} \right] \approx 0$, i.e., the nucleus-electron correlation becomes much weakened.

The nuclear wavefunction in Eq. (10) is numerically represented in a discrete variable representation (DVR), e.g., on a set of uniform grid points on which Fourier Grid Hamiltonian^{62,63} (FGH) is fully diagonalized. When the nuclear wavefunction $\chi(\mathbf{R})$ becomes oscillatory, for instance, for excited vibrations, the nodes at which $\chi(\mathbf{R}_{\text{nodes}}) = 0$ pose strong singularities in the embedding potential $\mathbf{V}^{\text{cp}}(\chi)$ that creates derivative discontinuities (i.e., cusps) in $\psi_i(\mathbf{r}, \mathbf{R}_{\text{nodes}})$ and singularities in $E_{el}(\mathbf{R}_{\text{nodes}})$ through Eq. (9). To circumvent this problem, we solve Eqs. (9) and (10) piecewisely according to the node positions of χ ; on the other hand, the proximal region of $\chi(\mathbf{R}_{\text{nodes}}) = 0$ is where nucleus-electron correlations are deemed strong.^{58,64}

The SCF procedure of NECSCF implementation is depicted in Fig. 1. The initial electronic orbitals are taken from standard BO Hartree-Fock MOs. An initial nuclear wavefunction is constructed on the uniform grid points of selected nuclear modes and computed using FGH solver for the initial BO PES. We adopt a two-step optimization in which microiteration cycles for electronic wavefunction are carried out in the presence of $\frac{\nabla_v \chi}{\chi}$ solved from the previous NECSCF macroiteration. The NECSCF convergence can be usually achieved in a reasonable number of iterations for small molecules reported in this work (see Fig. 2 for numerical demonstration).

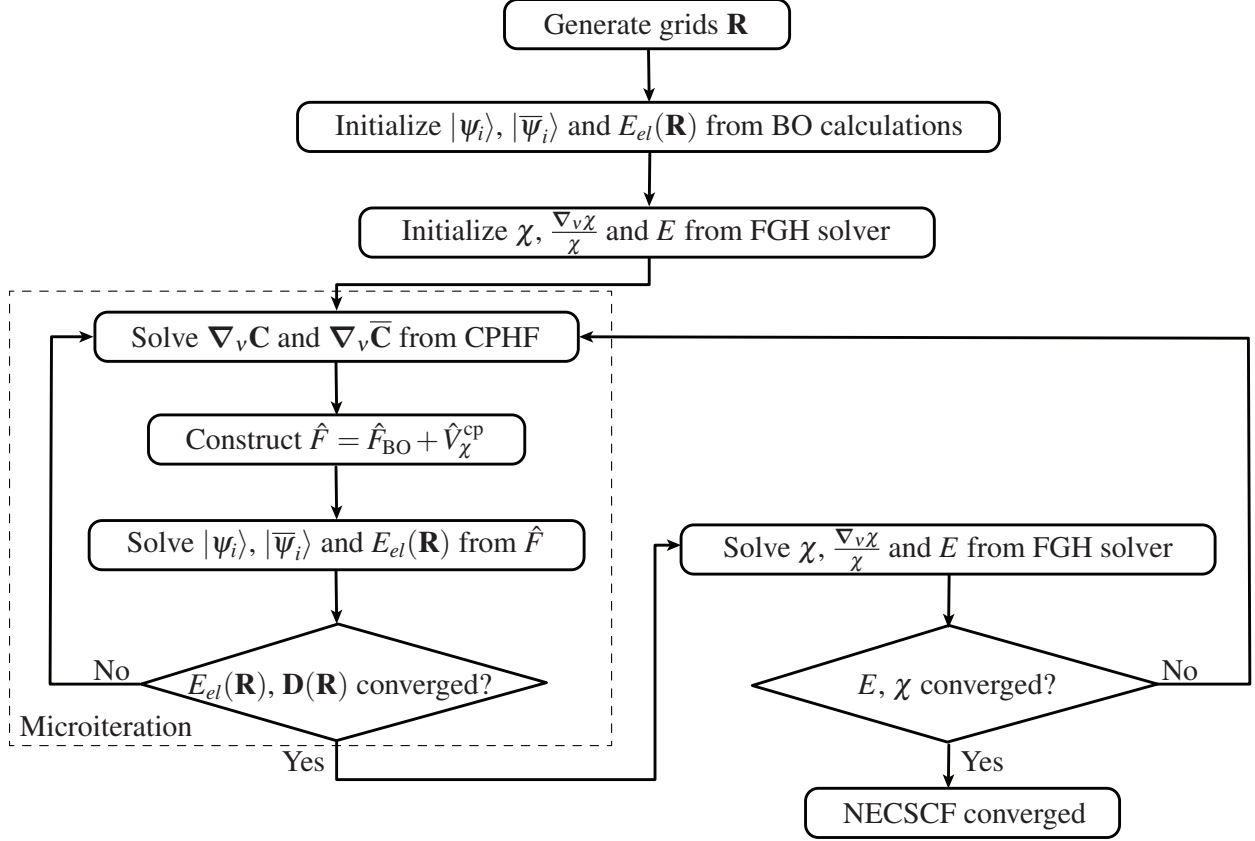


FIG. 1. The SCF iteration in NECSCF implementation. The electronic microiteration computes and converges $E_{el}(\mathbf{R})$, the electronic density matrix $\mathbf{D}(\mathbf{R})$ and the embedding potential in the presence of $\frac{\nabla_v \chi}{\chi}$ resulting from the nuclear equation that is solved in the previous macroiteration. Each microiteration solves both NECSCF-based Hartree-Fock and coupled perturbed Hartree-Fock equations iteratively, and macroiteration computes the molecular energy by exact diagonalization. This two-step optimization proceeds until the numerical convergence of both electronic and molecular energies within specified criteria.

E. Relation to variational search of exactly factorized wavefunction

Having introduced the NECSCF method, one fundamental and interesting question would be to ask whether, in principle, such an exact solution exists for a system of coupled electrons and vibrations. It can be proved that the minimization search for optimal Slater determinant for the self-consistently coupled electronic and nuclear equations does exist, however, on three stationary conditions of the molecular energy with respect to variations of electron density, nuclear wavefunction and paramagnetic current density ($\mathbf{j}(\mathbf{r}, \mathbf{R})$).⁵¹ While the NECSCF equations can be solved for the conditional electronic wavefunction and marginal nuclear wavefunction variationally, the

last condition requires the direct minimization of the energy with respect to paramagnetic current density to uniquely determine the geometric vector potential $\mathbf{A}_{00}^{(v)}$ and to account for induced electromagnetic interactions with nuclei. Our NECSCF procedure leaves a freedom to choose $\mathbf{A}_{00}^{(v)}$ from solving electronic and nuclear equations, and we have discussed (Section II C) to fix this freedom by making the gauge choice of $A_{ii}^{(v)} = 0$ via a geometric relaxation of the occupied NECSCF MOs. As a proxy to the third stationary condition, this choice equally vanishes the paramagnetic current density as $\mathbf{j}(\mathbf{r}, \mathbf{R}) \sim \text{Im tr}(\mathbf{A}_{00}^{(v)})$ for Slater determinant wavefunction.

The impact of $\mathbf{j}(\mathbf{r}, \mathbf{R})$ (or vector potential $\mathbf{A}_{00}^{(v)}$) can be understood from the effective coupled equations (Eqs. (B2) and (B5) in Appendix B). The effective nuclear kinetic energy operator \hat{T}_n (Eq. (B6)) defines the kinetic energy of electronically coupled nuclei that appear to move on an effective electronic potential surface $\tilde{E}_{el}(\mathbf{R})$ governing the effective nuclear equation Eq. B5, as opposed to the original nuclear equation (Eq. (A3)).

III. COMPUTATIONAL DETAILS AND EFFICIENCY

All electronic structure computations presented in this work were performed using cc-pVTZ basis set for non-H atoms and aug-cc-pVTZ for H except for basis set convergence tests. Our NECSCF program is interfaced with the PySCF program package⁶⁵ for accessing to one- and two-electron integrals and their derivatives. The nuclear wavefunction was constructed on the grid points that are evenly spaced 0.005 Å apart and sufficiently wide such that the tail of resulting nuclear amplitudes decays below 10^{-5} au. For instance, 321 and 241 grid points were used for the ground vibrational level of H_2^+ and H_2 , respectively. For molecules that contain heavy atoms, the number of grid points required is smaller than that for H_2^+ and H_2 . To reduce wall-clock time, the parallel computing was enabled by allocating electronic SCF calculation on each nuclear grid to individual process within the microiteration.

The iterative absolute energy updates are shown in Fig. 2 between two successive macroiterations for H_2 and HF molecules. For such a very simple H_2 molecule, the molecular energy E converges in 2 macroiterative cycles for vibrational ground and that for $v = 1$ level requires one more macroiteration to meet the convergence threshold. Without enabling the microiteration of $E_{el}(\mathbf{R})$, it takes 9 and 10 cycles to converge E for electrons coupled with $v = 0$ and $v = 1$ vibration, respectively. The coupling term $\frac{\nabla_v \chi(\mathbf{R})}{\chi(\mathbf{R})}$ is numerically ill-defined at the nodes of $\chi(\mathbf{R})$. Therefore, the PES $E_{el}(\mathbf{R})$ is generally more difficult to converge for excited nodal vibrational

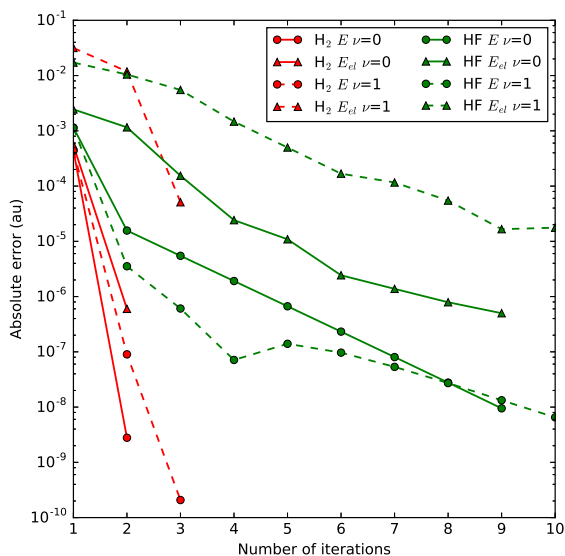


FIG. 2. Comparisons of the NECSCF energy convergence performance (macroiteration) of the total molecular energy (E) and non-BO electronic PES ($E_{el}(\mathbf{R})$) for H_2 and HF at $\nu = 0, 1$ vibrational levels. The NECSCF is converged when the change of E is within 10^{-8} au in the macroiteration. The convergence criterion for the electronic microiteration is met if the minimal change of the electronic energy is below 10^{-4} au or the maximal number of micro-iterations exceeds 20. The absolute energy change (au) shows energy updates of ΔE (filled circle) and the maximal $\Delta E_{el}(\mathbf{R})$ (filled triangle) amongst all grid points between two successive macroiteration cycles.

wavefunction $\chi(\mathbf{R})$. For instance, the electronic energy $E_{el}(\mathbf{R})$ for $\nu = 1$ level of H_2 shows a large numerical variation and instability at an order of DBOC correction at a bond distance very close to the node, even the convergence of the molecular energy E is well achieved. The significant error in E_{el} has very limited influence on the convergence of E because nuclear density is negligible at nodes and tails. The similar convergence pattern is observed for HF molecule. The $\nu = 0$ energies E and E_{el} are converged within 10^{-8} and 5×10^{-7} au in 9 macroiterations. However, for each macroiteration, 3 microiterations are needed on the average. In case of $\nu = 1$, up to 17 microiterations are required to converge E_{el} within 10^{-4} in the vicinity of node. Without using the microiteration, the number of iterative cycles increases to 24 and 26 for $\nu = 0$ and $\nu = 1$ vibration, respectively.

IV. RESULTS

A. Molecular energetics

The NECSCF-based binding energies of H_2 molecules (H_2 , HD and D_2) and their cations (H_2^+ , HD^+ and D_2^+) were obtained from the eigenvalue difference of the nuclear equation Eq. (10) governing nuclear motion, as shown in Fig. 3 for various basis sets. For cations, highly accurate

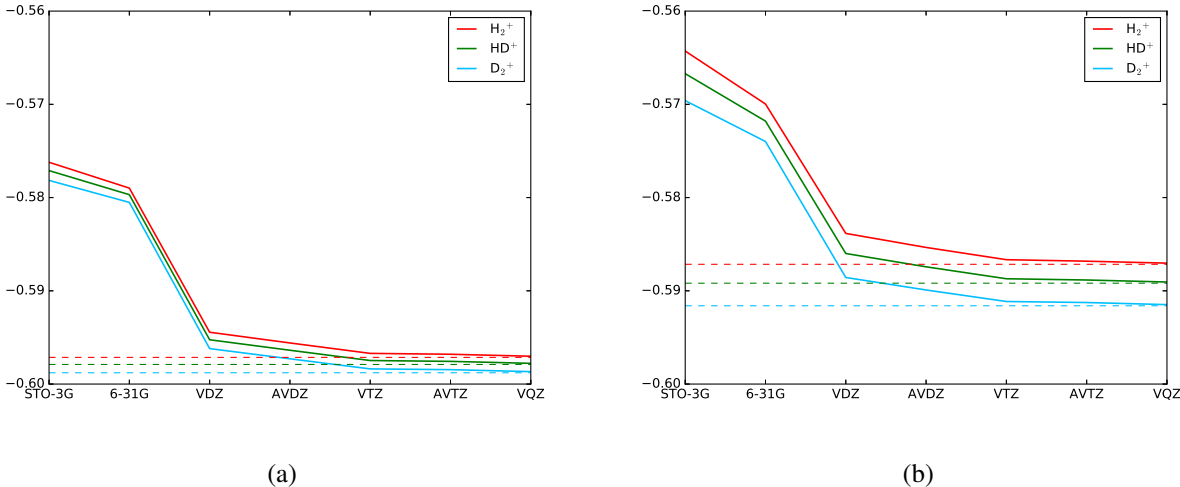


FIG. 3. Comparison of the binding energy (au) convergence for H_2^+ , HD^+ and D_2^+ at $v=0$ (a) and $v=1$ (b) vibrational level using a range of basis sets. The reference data from nonadiabatic variational results⁶⁷ are given in dashed lines.

reference values have been reported in studies using nonadiabatic variational^{67,68} and QMC⁶⁹ methods which benchmark non-BO energy corrections for these molecules exhibiting no electronic correlation. The NECSCF results of VXZ ($X=T, Q, 5$) basis sets were extrapolated^{70,71} to obtain the complete basis set (CBS) limits, as given in Table I. The details of CBS extrapolation can be found in Table S2 and S3 of the Supplementary Materials. The absolute errors of the uncorrelated NECSCF binding energies are in an order of 10^{-6} - 10^{-8} au, indicating a promising agreement to the benchmark data. The non-BO energy corrections to the conventional BO values are around 10^{-4} au, which are 2–3 orders of magnitude greater than the energy deviations from the benchmark.

For correlated H_2 molecule, the electronic correlation is of essential significance. The CBS limits at NECSCF, NECSCF-MP2 and NECSCF-FCI level of theory are -1.12284883, -1.15726946 and -1.16406555 au, respectively. Obviously, the electronic correlation correction at the FCI level

TABLE I. Comparison of the CBS limits between the BO and non-BO FCI binding energies (ΔE , au). The NECSCF nucleus-electron couplings with $\nu = 0$ and $\nu = 1$ vibrational levels were included for H_2^+ , HD^+ , D_2^+ and H_2 . The reference data from the nonadiabatic variational method are provided for comparison⁶⁷.

Binding energy (ΔE)	H_2^+	HD^+	D_2^+	H_2
$\nu = 0$				
BO-FCI	-0.59739883	-0.59809351	-0.59891992	-1.16452199
NECSCF-FCI	-0.59714185	-0.59790031	-0.59879051	-1.16406555
Ref.	-0.59713906 ^c	-0.59789797 ^c	-0.59878878 ^c	-1.16402502 ^d
non-BO correction ^a	0.00025698	0.00019320	0.00012941	0.00045644
non-BO error ^b	0.00000279	0.00000234	0.00000173	0.00004053
$\nu = 1$				
BO-FCI	-0.58741083	-0.58937451	-0.59173259	-1.14555622
NECSCF-FCI	-0.58715734	-0.58918220	-0.59160316	-1.14510815
Ref.	-0.58715568	-0.58918183	-0.59160312	-1.14506537 ^e
non-BO correction ^a	0.00025349	0.00019231	0.00012943	0.00044807
non-BO error ^b	0.00000166	0.00000037	0.00000004	0.00004278

^a $|\Delta E_{\text{NECSCF-FCI}} - \Delta E_{\text{BO-FCI}}|$.

^b $|\Delta E_{\text{NECSCF-FCI}} - \Delta E_{\text{ref.}}|$.

^c From ref. 67.

^d From ref. 72.

^e From ref. 73.

is a prerequisite to the successful recovery of the benchmark value -1.16402502 au ⁷² from which our NECSCF-FCI deviates by only 0.04 mau, an order of magnitude smaller than the nucleus-electron correction of 0.46 mau to the binding energy. The NECSCF-MP2 ($\nu=0$) and NECSCF-FCI ($\nu=0$) electron correlation energy is -0.03442063 and -0.04121672 au in the presence of the explicit nucleus-electron coupling, as compared to the BO-MP2 and BO-FCI electron correlations of -0.03441996 and -0.04121423 au, respectively. As such, for H_2 molecule, the non-BO corrections to electron correlation are only about 0.2 cm^{-1} and -0.5 cm^{-1} from NECSCF-MP2 and NECSCF-FCI correlated models, respectively, which makes a negligible contribution to the overall non-BO correction that must be dominated by the NECSCF nucleus-electron coupling among

mean-field electrons.

Next, we assess the non-BO energy corrections from NECSCF and NECSCF-MP2 computations for many-electron hydride molecules (Table II) by comparing to reported FN-DMC¹⁹ results. Our NECSCF-MP2 energy corrections for most hydrides deviate from FN-DMC reference within 0.5 mau (1.3 kJ/mol), and the inclusion of MP2 correlations largely decreases the energy error. The discrepancy of NECSCF corrections from the additive correction by the zero-point energy (ZPE) and DBOC can be viewed as contribution beyond the limit of BO electronic states, including nucleus-electron correlation effects on modifying electronic potential, ZPE and DBOC. The remaining non-BO correction is > 0.2 mau for BH, CH ($^4\Sigma$) and HF. In general, it is noted that most of the nucleus-electron couplings are promisingly captured at the mean-field NECSCF level. However, a relatively large discrepancies of 2.4 mau (6.3 kJ/mol) and 1.8 mau (4.7 kJ/mol) occur to the doublet CH ($^2\Pi$) and quartet CH ($^4\Sigma$) states, respectively, probably due to their strong multi-reference characters for which the electronic correlation at MP2 level is insufficient. The implementation of NECSCF-based multi-state multi-reference correlation methods such as NECSCF-CASSCF and NECSCF-NEVPT2 (NECSCF-based N-electron Valence State Perturbation Theory) will be reported in future.

TABLE II. Non-BO energy corrections (mau) to first-row hydrides.

Molecule	NECSCF	NECSCF-MP2	FN-DMC ^a	ZPE+DBOC ^a
LiH	4.09(6)	4.14(5)	4.28(3)	4.07(2)
BeH	5.71(6)	5.76(0)	5.99(6)	5.90(1)
BH	7.25(0)	7.29(1)	7.39(9)	7.03(2)
CH ($^2\Pi$)	8.50(4)	8.37(5)	10.8(3)	8.54(9)
CH ($^4\Sigma^-$)	9.29(4)	9.03(9)		
OH	11.5(7)	11.1(2)	11.1(5)	11.1(0)
HF	12.8(8)	12.3(7)	12.0(4)	12.1(4)

^a From ref. 19

The NECSCF and NECSCF-MP2 proton affinities (PAs) of five diatomic molecules were calculated using the procedure described in Ref. 34, and are compared with the experimental⁷⁴, NEO-HF and NEO-OOMP2³⁴ values. For the calculation of protonated species, all vibrational modes (3 for non-linear and 4 for linear triatomic molecules) were selected to couple individually with

electronic MOs, whereas only the results with the modes yielding the smallest absolute error from experimental data are presented in Table III. The PAs associated with the remaining molecular vibrations are provided in Table S1 of the Supplementary Materials. NECSCF-based methods achieve the best performance for the asymmetric proton stretching of H-XY molecule, where the proton departure from XY⁻ decreases the X-Y bond length. This is consistent with the relatively shorter equilibrium bond distance in XY⁻ than in H-XY molecule. The absolute error of NECSCF is generally smaller than NEO-HF since the nuclear anharmonic motion and ZPE are exactly incorporated through FGH solution. NECSCF-MP2 is also able to achieve a comparable accuracy to the NEO-OOMP2 values.

TABLE III. Absolute deviations (eV) of the PAs from experimental data.

Molecule	Experiment ^a	NECSCF	NEO-HF ^b	NECSCF-MP2	NEO-OOMP2 ^b
CN ⁻	15.31	0.20	0.91	0.34	0.29
N ₂	5.12	0.00	0.76	0.03	0.23
HS ⁻	15.31	0.25	0.84	0.29	0.31
OH ⁻	16.95	0.50	0.36	0.07	0.42
CO	6.16	0.02	0.84	0.10	0.04

^a From ref. 74.

^b From ref. 34.

B. Bond length

BO quantum chemistry methods associate equilibrium molecular structures with the energy minima on the PES of molecule. However, the presence of ZPE, anharmonic vibrations and non-BO couplings necessitates the determination of vibrationally averaged properties to reflect the thermal nature of atomic positions.^{75,76} Here, we demonstrate the NECSCF computation of vibrationally averaged bond lengths $\langle R \rangle$ and the non-BO impact for typical diatomic and triatomic molecules, according to the expectation value of the single product molecular wavefunction fulfilling PNC condition.

$$\langle R \rangle = \langle \Psi(\mathbf{rs}, \mathbf{R}) | \mathbf{R} | \Psi(\mathbf{rs}, \mathbf{R}) \rangle_{\mathbf{rsR}} = \langle \chi(\mathbf{R}) | \mathbf{R} | \chi(\mathbf{R}) \rangle_{\mathbf{R}} \quad (40)$$

The NECSCF and NECSCF-MP2 results averaged on the ground $\nu = 0$ and first excited $\nu = 1$ vibrational modes are compared with the full-quantum cNEO-DFT³⁷ and experimental values in Table IV.

For all computed chemical bonds involving H atom, it can be seen that the non-BO nucleus-electron coupling effects lead to a notable increase of equilibrium bond length. In contrast, for the bonds between heavier atoms, the non-BO coupling with $\nu = 0$ vibration leads to the bond length elongation of only $\sim 0.01 \text{ \AA}$ for D-F, D-C, D-N and D-O bonds and $< 0.005 \text{ \AA}$ for C-N bonds, respectively, as compared to both BO RHF and MP2 results. The $\nu = 1$ vibration results in further expansion of atomic positions and longer averaged bond lengths than those with $\nu = 0$. It is also observed that deuteration shortens both NECSCF and NECSCF-MP2 bond lengths. For instance, the H-F bond length is larger than D-F by 0.004 \AA . The isotopic effect influences the non-BO bond length by both electronic and vibrational factors: on one hand, the significance of the nucleus-electron coupling for electronic motion decreases with increasing atomic mass. On the other hand, large atomic mass tends to narrow the landscape of nuclear wavefunction, which leads to a decrease of averaged bond length. Finally, the average bond lengths at the NECSCF-FCI level were further computed for H_2 molecules. The comparison with NECSCF and NECSCF-MP2 are presented in Fig. 4. Among the hydrogen molecules, H_2 has the largest bond length increase,

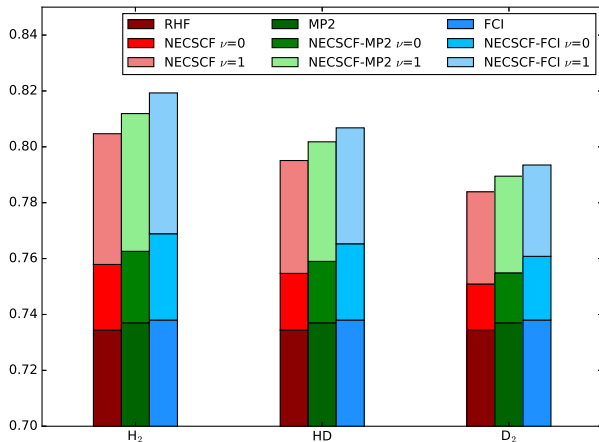


FIG. 4. Vibrationally averaged bond lengths (\AA) of H_2 .

whereas the change of D-D interatomic distance is the smallest.

TABLE IV. Vibrationally averaged bond lengths (\AA) of selected molecules at $\nu = 0$ and $\nu = 1$ vibrational levels. For computed bond lengths of triatomic molecules, only the bond stretching mode of interest is active with other modes frozen. For comparisons, the regular equilibrium RHF and MP2 bond lengths are equivalent to vibrational averages in the BO harmonic potential; the experimental bond lengths were determined by fitting the BO spectroscopic constants which lead to the same geometric parameters for all isotopomers.

Molecule	Bond	Experiment ^a	RHF	NECSCF		MP2	NECSCF-MP2		cNEO-DFT ^b
				$\nu = 0$	$\nu = 1$		$\nu = 0$	$\nu = 1$	
H ₂	H-H	0.7414	0.7344	0.7579	0.8047	0.7370	0.7626	0.8119	0.785
HD	H-D	0.7414		0.7547	0.7951		0.7590	0.8018	0.779
D ₂	D-D	0.7415		0.7509	0.7839		0.7549	0.7895	0.760
HF	H-F	0.9168	0.8979	0.9121	0.9371	0.9169	0.9318	0.9528	0.942
DF	D-F			0.9083	0.9292		0.9281	0.9501	0.937
HCN	C-H	1.064	1.0570	1.0709	1.0954	1.0599	1.0737	1.0980	1.089
	C-N	1.156	1.1337	1.1369	1.1431	1.1808	1.1850	1.1922	1.147
DCN	D-C			1.0671	1.0869		1.0697	1.0901	1.082
	C-N			1.1368	1.1429		1.1850	1.1922	1.147
HNC	N-H	0.986	0.9830	0.9968	1.0223	0.9921	1.0067	1.0316	1.019
	C-N	1.173	1.1558	1.1592	1.1660	1.1909	1.1951	1.2026	1.165
DNC	D-N			0.9930	1.0128		1.0027	1.0226	1.012
	C-N			1.1592	1.1659		1.1950	1.2025	1.165
H ₂ O	H-O	0.958	0.9406	0.9552	0.9847	0.9560	0.9716	1.0031	0.981
HDO	H-O	0.956		0.9552	0.9846		0.9716	1.0030	0.982
	D-O	0.956		0.9512	0.9725		0.9672	0.9899	0.975
D ₂ O	D-O	0.956		0.9511	0.9723		0.9672	0.9898	0.975

^a From ref. 77.

^b From ref. 37.

C. Nuclear and electron density

In this section, we exam the non-BO effects on the nuclear and electronic density distribution. At our disposal, the NECSCF method discards molecular translational and rotational motions. The nuclear density $P_\nu(\mathbf{R})$ only depends on the interatomic distance \mathbf{R} of diatomic molecules and the excitation level ν of the nuclear wavefunction χ_ν . Here, we define the non-BO correction to nuclear density $\Delta P_\nu(\mathbf{R})$ as

$$\Delta P_\nu(\mathbf{R}) = P_\nu^{\text{NECSCF}}(\mathbf{R}) - P_\nu^{\text{HO}}(\mathbf{R}) \quad (41)$$

with

$$P_\nu^{\text{NECSCF}}(\mathbf{R}) = \chi_{\nu,\text{NECSCF}}^\dagger(\mathbf{R})\chi_{\nu,\text{NECSCF}}(\mathbf{R}), \quad (42)$$

$$P_\nu^{\text{HO}}(\mathbf{R}) = \chi_{\nu,\text{HO}}^\dagger(\mathbf{R})\chi_{\nu,\text{HO}}(\mathbf{R}) \quad (43)$$

where $\chi_{\nu,\text{NECSCF}}$ is the nuclear probability amplitude calculated from NECSCF PES and $\chi_{\nu,\text{HO}}$ the quantum harmonic oscillator (HO) function for the ν -th vibrational level. The non-BO density corrections for two low-lying states [$\Delta P_0(\mathbf{R})$ and $\Delta P_1(\mathbf{R})$] for H_2 , HF and their isotopes are graphed in Fig. 5. Specifically, the non-BO correction $\Delta P_{\nu=0}(\mathbf{R})$ transfers the nuclear density

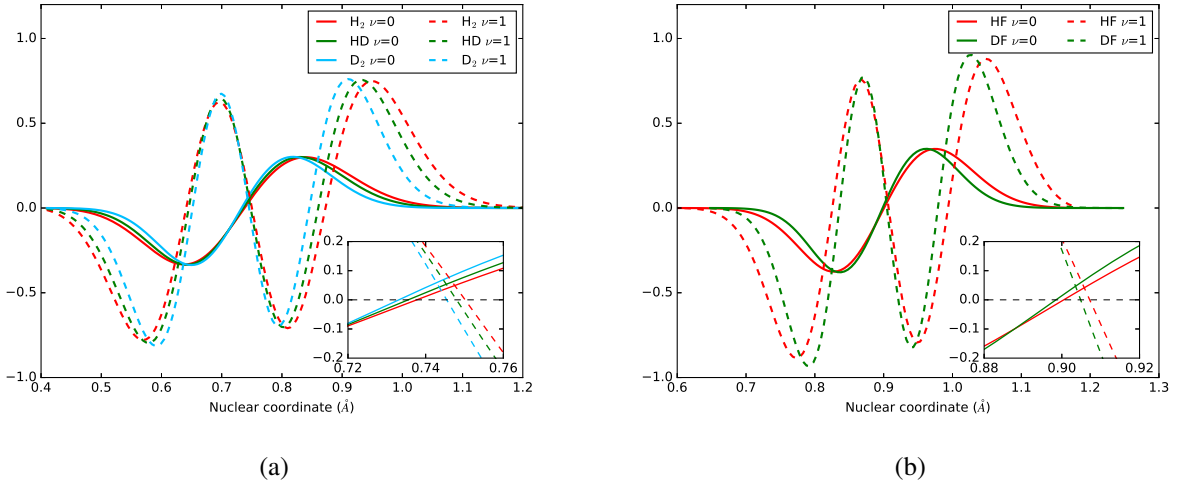


FIG. 5. The NECSCF correction (au) to quantum HO nuclear density of H_2 (a) and HF (b). The inset shows the details around the equilibrium bond lengths.

from the short bond region to the long bond region, e.g., from 0.4–0.7 Å to 0.7–1.2 Å for H_2 . This actually reveals an increase of the vibrationally averaged bond length for both H_2 and HF, which is consistent with the results presented in previous section. $\Delta P_{\nu=1}(\mathbf{R})$ is apparently much stronger

than $\Delta P_{v=0}(\mathbf{R})$, which is also in line with the bond elongation as shown in Fig. 4. Moreover, the deuteration, which involves heavier atoms and diminishes the nucleus-electron coupling, shifts the nuclear density more significantly towards the equilibrium bond region. This results in less bond elongation with more deuteration, following the same isotopic effect as the averaged bond distance in the order of $D_2 < HD < H_2$ and $DF < HF$.

Based on the idea of the dynamic distribution of electron density⁷⁸, we characterize the non-BO correction ($\langle \Delta \rho \rangle_v$) to the dynamic electron density as,

$$\langle \Delta \rho \rangle_v = \langle \rho \rangle_{v, \text{NECSCF}} - \langle \rho \rangle_{v, \text{HO}} \quad (44)$$

and the z -component of $\langle \Delta \rho \rangle_v$ in the direction of molecular axis

$$\langle \Delta \rho \rangle_v^z = \int \int dx dy \langle \rho \rangle_v. \quad (45)$$

Here, $\langle \rho \rangle_{v, \text{NECSCF}} = \int d\mathbf{R} \rho P_v^{\text{NECSCF}}(\mathbf{R})$ and ρ is the electron density from NECSCF computation. $\langle \Delta \rho \rangle_0^z$ and $\langle \Delta \rho \rangle_1^z$ for H_2 are shown in Fig. 6a.

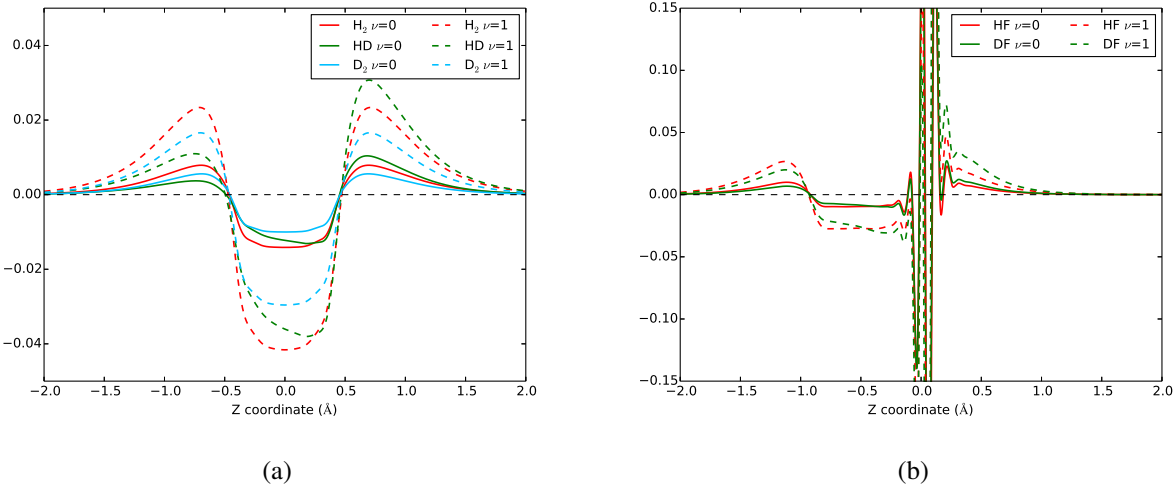


FIG. 6. The z -component of dynamic electron density corrections (au) of H_2 (HD and D_2) **(a)** and HF (DF) **(b)**. z represents the molecular axis.

Upon the nucleus-electron coupling, symmetric density transfer takes place from the interstitial bonding region between atoms to the peripheral region in H_2 and D_2 . Due to the decreased nuclear quantum effect with heavier isotopes, the electron density transfer is obviously less significant in D_2 than H_2 . For heteronuclear HD, the dynamic electron transfer becomes asymmetric. Moreover, it is observed that the transfer of electron density is highly directional from the bonding to the

surrounding area. As illustrated from the yz -contour of $\langle \Delta \rho \rangle$ (Fig. 7), the non-BO construction

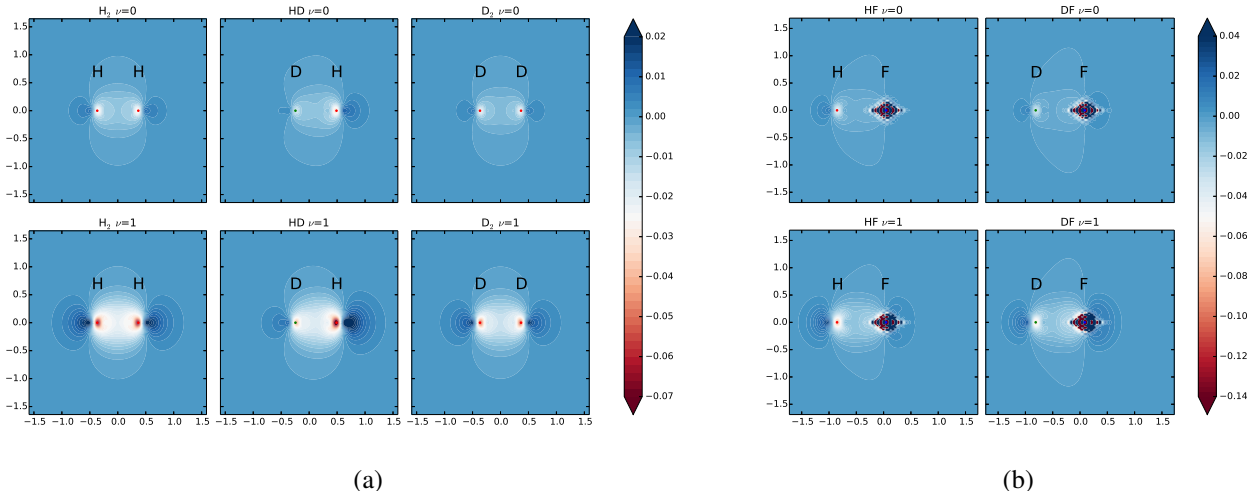


FIG. 7. The yz -contour of dynamic electron density corrections (au) of H_2 (HD and D_2) **(a)** and HF (DF) **(b)**.

of electron density is much stronger along the z -direction in which H-H vibrates than in other orientations, which thus weakens and elongates the σ -bond. The $\nu = 1$ level of vibration appears to further enhance the density transfer that follows a similar pattern with that for $\nu = 0$ and leads to even longer bond lengths. For HF molecule, however, an intensively local variation of electron density is observed in the near proximity of F atom which possesses strong electronegativity, and becomes much more local than H_2 . Nonetheless, more electron density destruction can be still discernible in the F atom’s bonding region than the opposite side.

D. FHF⁻ molecule

As an illustrative application of our NECSCF and NECSCF-MP2 implementations, we demonstrate the nucleus-electron effect on FHF⁻ molecule for which the paradigmatic proton-electron coupling has been well studied in literature. The computed NECSCF and NECSCF-MP2 PESs incorporating the nucleus-electron coupling individually with $\nu = 0$ and $\nu = 1$ proton shuttle mode are shown in Fig. 8 where the non-BO behavior is compared with standard RHF PES. The difference in minimal energy for F-F lengths between NECSCF ($\nu=0$) and standard RHF was computed to be 0.026 \AA which is in excellent agreement with reported 0.02 \AA arising from the proton quantum effect³³. Interestingly, although the electronic correlation elongates F-F bond, the change

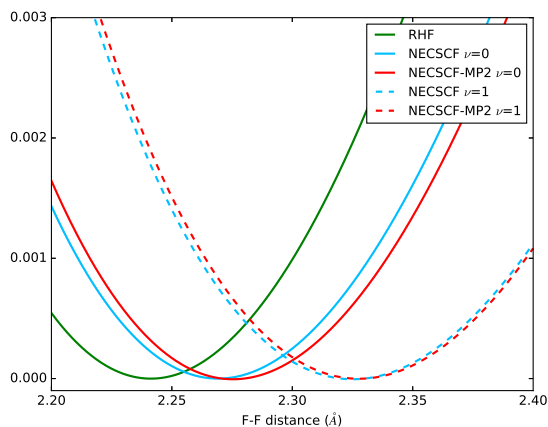


FIG. 8. Comparison of the PES as a function of F-F distances for FHF^- between standard RHF, NECSCF and NECSCF-MP2 computations. The energy minima of all curves are shifted for comparison convenience.

made by MP2 correlation is not as significantly strong as the proton quantum effect.

Using the tool we developed in previous section, the nuclear and electron density analyses for the proton quantum effect are shown in Fig. 9. In consistence with the NEO-DFT prediction⁷⁹,

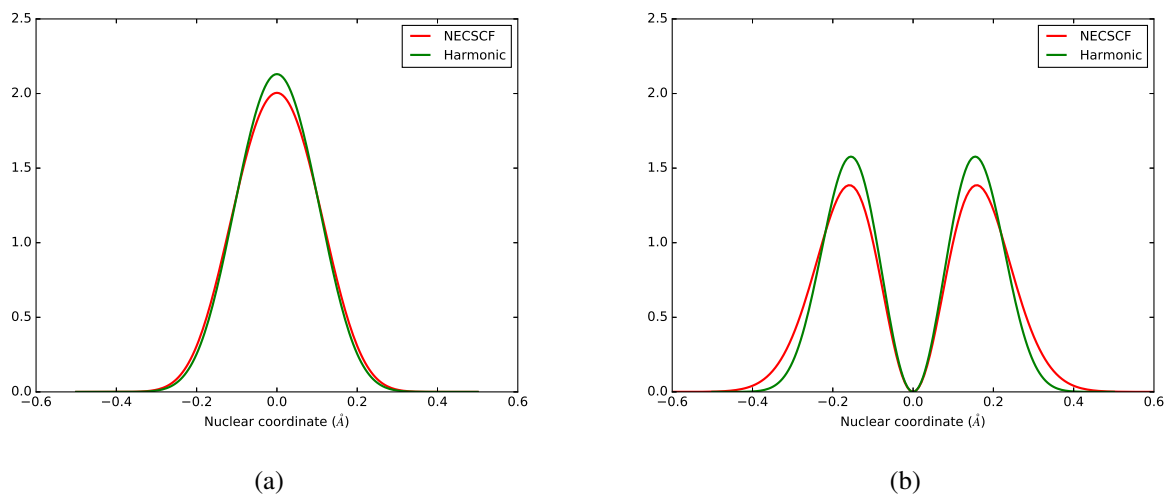


FIG. 9. NECSCF and harmonic protonic density (au) of FHF^- for $\nu=0$ (a) and $\nu=1$ (b) vibrational levels. The vibrational frequency of the quantum HO is obtained from RHF calculation. The F-F distances are determined according to the PES minima for NECSCF and RHF, respectively.

the majority of the protonic density at $\nu = 0$ vibrational state lies in a range of -0.3 – 0.3 Å. As compared to harmonic result, the peak of the NECSCF protonic density decreases with slightly

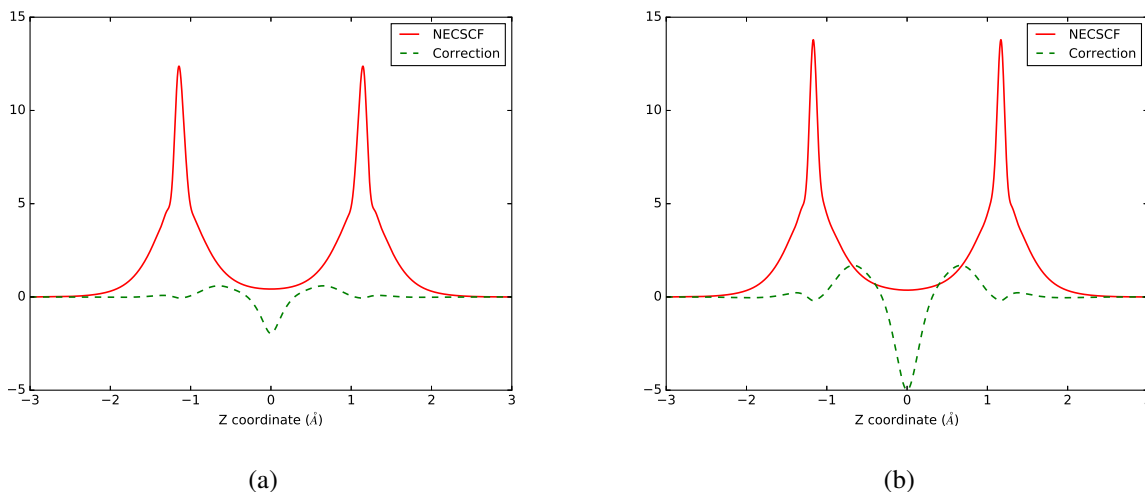


FIG. 10. The z -component of NECSCF dynamic electron density (au) of FHF^- for $v=0$ (a) and $v=1$ (b) vibrational levels. The correction to the electron density is magnified by 100 times to exhibit the protonic non-BO significance. The F-F distance is determined according to the NECSCF PES minimum.

broadened distribution width, and the tail decay of the NECSCF density is relatively slower than the RHF one. These subtle changes should be attributed to the inclusion of the nucleus-electron coupling. The first excited $v = 1$ protonic density exhibits changes in a similar fashion with $v = 0$, but with greater density broadening. For electron density distribution (Fig. 10), the correction to the dynamic density is rather small, primarily due to the low electron density on the proton and strongly electronegative F atoms. The density correction is symmetric as anticipated, and the density transfers from the equilibrium proton position towards both left and right H-F bonding regions.

In Fig. 11 we present the slices of three-dimensional (3D) NECSCF protonic difference density from the RHF reference. This quantity measures the response of protonic density from the non-BO NECSCF correction for FHF^- at $v = 0$, for which the NECSCF energy correction is computed to be 1.1 mau. Due to the rotational shape, the result for y -component is the same as x . As opposed to Fig. 9, the non-BO NECSCF effect slightly enhances the protonic density around the equilibrium position ($-0.15 \text{ \AA} - 0.15 \text{ \AA}$) and depletes in the remaining region along the molecular axis. At $v = 1$, a nodal point appears at the equilibrium position, and the protonic density enhancement area extends to $-0.2 \text{ \AA} - 0.2 \text{ \AA}$. The x -component does not show proton depletion at $n = 0$, and it is constantly 0 since $v = 1$ 3D proton density exhibits xy nodal plane at the equilibrium position. Interestingly, the one-dimensional (1D) nuclear difference density computed by confining

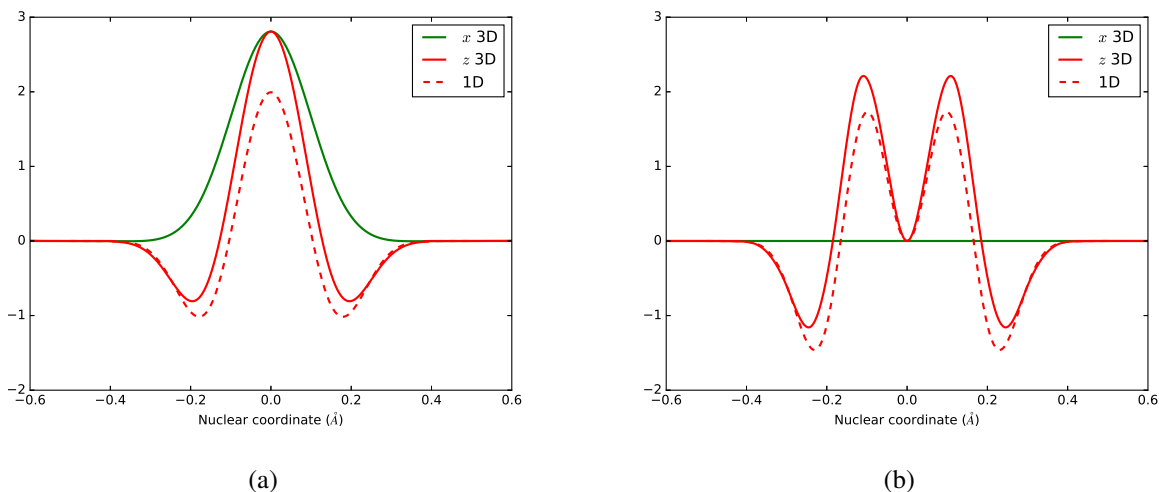


FIG. 11. The x and z -component of 3D NECSCF corrections to RHF protonic density (mau) of FHF^- for $\nu=0$ **(a)** and $\nu=1$ **(b)** vibrational levels. The 1D corrections along z -direction is computed by freezing the x - and y -directions. The root-mean-square deviations in the proton density over 3D space are 0.19 and 0.14 mau for $\nu = 0$ and $\nu = 1$, respectively. The RHF protonic density is calculated using the BO RHF PES. The F-F distances are determined according to the PES minima for NECSCF and RHF, respectively. The z -component is along with the molecular axis whereas x direction is perpendicular to the molecular axis.

the protonic motion to z -direction demonstrates very similar patterns with the z -component of 3D correction. For polyatomic molecules with multiple vibrational degrees of freedom, the nucleus-electron coupling behavior of individual mode can be examined by selecting the nuclear motion that makes the most significant contribution to the non-BO correction.

V. CONCLUSIONS

The significance of non-BO effects involving nucleus-electron correlated motion is manifested in many chemistry problems that are difficult for traditional quantum chemistry methods within the BO framework. We have developed an NECSCF method for conveniently treating the nucleus-electron coupling using an exact factorization of the molecular wavefunction. The working equations for the nuclear and electronic subsystems are derived and implemented currently for uncorrelated electronic ground state for which the NECSCF theory is exact and invariant to unitary orbital rotation, with the particular choice of geometric gauge transformation that yields an anti-symmetric derivative vector potential. The post-HF electronic correlation can be computed

by using resulting NECSCF MOs, as demonstrated to MP2 and FCI correlation methods. The computations of vibrationally averaged properties, including molecular energy, bond length, electronic and nuclear density are demonstrated and compared. The NECSCF predicts that nucleus-electron coupling generally weakens the bonding strength and favors bond elongation, as well as an electron density transfer out of the bonding area along the vibrational progression in which the nucleus-electron coupling takes place. The present work not only provides an alternative computational approach for accurately treating non-BO problems, but also lays the basis for a general methodological framework in which systematic methods can be developed for nucleus-coupled strongly correlated electrons and excited electronic states on multiple PESs from NECSCF mean-field wavefunction in our future endeavor.

SUPPLEMENTARY MATERIAL

The supplementary material contains data for proton affinities and basis set limit extrapolation results for H_2^+ , HD^+ , D_2^+ and H_2 .

ACKNOWLEDGMENTS

We acknowledge the funding support from the Seed Fund Program for Basic Research (Grant No. 201711159116) by the University of Hong Kong and the Computational Initiative provided by the Faculty of Science at HKU. J.Y. acknowledges the research program of AIR@InnoHK cluster from the Innovation and Technology Commission of Hong Kong SAR of China. The computations were partially performed using research computing facilities offered by Information Technology Services, the University of Hong Kong. We are grateful to Professor Sharon Hammes-Schiffer for helpful discussions and comments.

DATA AVAILABILITY STATEMENT

The data that supports the findings of this study are available within the article and its supplementary material.

Appendix A: Derivation of form-invariant NECSCF electronic and nuclear equations

The total molecular energy functional \mathcal{L} in terms of $\Phi(\mathbf{r}\mathbf{s}, \mathbf{R})$ and $\chi(\mathbf{R})$, subject to the normalization conditions in the electronic and nuclear coordinate space, is defined in Eq. (6). $\Phi(\mathbf{r}\mathbf{s}, \mathbf{R})$ here can be any type of electronic wavefunctions, not limited to the mean-field determinant. By variationally minimizing \mathcal{L} with respect to $\Phi(\mathbf{r}\mathbf{s}, \mathbf{R})$ and $\chi(\mathbf{R})$, the nonadiabatically coupled electronic and nuclear equations have been shown form-invariant under gauge transformation,^{50,51} but are not energy-invariant in general. In our approach, $\Phi(\mathbf{r}\mathbf{s}, \mathbf{R})$ is assumed as a Slater determinant and \mathcal{L} is minimized with respect to non-BO MOs $\psi_i(\mathbf{r}\mathbf{s}, \mathbf{R})$ to obtain the NECSCF electronic working equation. We adopt the spin orbital notation in the derivation and \mathbf{s} coordinate is dropped for simplicity. By evaluating $\langle \Psi(\mathbf{r}, \mathbf{R}) | \hat{H} | \Psi(\mathbf{r}, \mathbf{R}) \rangle_{\mathbf{r}}$, the energy functional \mathcal{L} in terms of non-BO spatial orbital $\psi_i(\mathbf{r}, \mathbf{R})$ and $\chi(\mathbf{R})$ reads,

$$\begin{aligned} \mathcal{L} = & \int d\mathbf{R} \chi^\dagger(\mathbf{R}) \chi(\mathbf{R}) \langle \Phi(\mathbf{r}, \mathbf{R}) | \hat{H}_{\text{BO}} | \Phi(\mathbf{r}, \mathbf{R}) \rangle_{\mathbf{r}} - \int d\mathbf{R} \sum_{\mathbf{v}} \frac{\chi^\dagger(\mathbf{R}) \nabla_{\mathbf{v}} \chi(\mathbf{R})}{M_{\mathbf{v}}} \sum_i \langle \bar{\psi}_i | \nabla_{\mathbf{v}} | \psi_i \rangle \\ & - \int d\mathbf{R} \chi^\dagger(\mathbf{R}) \chi(\mathbf{R}) \sum_{\mathbf{v}} \frac{1}{2M_{\mathbf{v}}} \left[\sum_i \langle \bar{\psi}_i | \nabla_{\mathbf{v}}^2 | \psi_i \rangle + \sum_i \sum_j \langle \bar{\psi}_i | \nabla_{\mathbf{v}} | \psi_i \rangle \cdot \langle \bar{\psi}_j | \nabla_{\mathbf{v}} | \psi_j \rangle \right. \\ & \left. - \langle \bar{\psi}_i | \nabla_{\mathbf{v}} | \psi_j \rangle \cdot \langle \bar{\psi}_j | \nabla_{\mathbf{v}} | \psi_i \rangle \right] + \int d\mathbf{R} \chi^\dagger(\mathbf{R}) \hat{T}_n \chi(\mathbf{R}) \langle \Phi(\mathbf{r}, \mathbf{R}) | \Phi(\mathbf{r}, \mathbf{R}) \rangle \\ & - \int d\mathbf{R} \sum_i \sum_j \tilde{\epsilon}_{ij}(\mathbf{R}) (\langle \bar{\psi}_i | \psi_j \rangle - \delta_{ij}) - E [\langle \chi(\mathbf{R}) | \chi(\mathbf{R}) \rangle_{\mathbf{R}} - 1]. \end{aligned} \quad (\text{A1})$$

The biorthogonality constrain $\langle \bar{\psi}_i | \psi_j \rangle - \delta_{ij} = 0$ ensures the PNC, and replaces the electronic normalization condition $\langle \Phi(\mathbf{r}, \mathbf{R}) | \Phi(\mathbf{r}, \mathbf{R}) \rangle_{\mathbf{r}} - 1 = 0$ in Eq. (6). The Lagrangian energy of Eq. (A1) is variationally minimized with respect to $\langle \bar{\psi}_i |$, $\chi(\mathbf{R})$, the multipliers $\tilde{\epsilon}_{ij}(\mathbf{R})$ and E , which leads to the NECSCF coupled electronic and nuclear equations as follows,

$$\left[\hat{F}_{\text{BO}} + \hat{V}_{\chi}^{\text{cp}} \right] | \psi_i \rangle = \frac{1}{|\chi(\mathbf{R})|^2} \sum_j \tilde{\epsilon}_{ij}(\mathbf{R}) | \psi_j \rangle, \quad (\text{A2})$$

$$\left[\hat{T}_n + \hat{E}_{el}(\mathbf{R}) \right] \chi = E \chi. \quad (\text{A3})$$

Above, the embedding operator $\hat{V}_{\chi}^{\text{cp}}$ is formally exact for uncorrelated electrons,

$$\hat{V}_{\chi}^{\text{cp}} = - \sum_{\mathbf{v}} \frac{1}{M_{\mathbf{v}}} \left(\frac{\nabla_{\mathbf{v}} \chi}{\chi} \cdot \nabla_{\mathbf{v}} + \frac{\nabla_{\mathbf{v}}^2}{2} + \sum_j \langle \bar{\psi}_j | \nabla_{\mathbf{v}} \psi_j \rangle \cdot \nabla_{\mathbf{v}} - |\nabla_{\mathbf{v}} \psi_j \rangle \cdot \langle \bar{\psi}_j | \nabla_{\mathbf{v}} \right). \quad (\text{A4})$$

In the nuclear equation, $\hat{E}_{el}(\mathbf{R})$ provides the NECSCF electronic potential operator,

$$\begin{aligned} \hat{E}_{el}(\mathbf{R}) = & \langle \Phi(\mathbf{r}, \mathbf{R}) | \hat{H}_{BO} | \Phi(\mathbf{r}, \mathbf{R}) \rangle_{\mathbf{r}} - \sum_{\mathbf{v}} \frac{1}{2M_{\mathbf{v}}} \sum_i \left(\langle \bar{\psi}_i | \nabla_{\mathbf{v}}^2 | \psi_i \rangle + 2 \langle \bar{\psi}_i | \nabla_{\mathbf{v}} | \psi_i \rangle \cdot \nabla_{\mathbf{v}} \right. \\ & \left. + \sum_j \langle \bar{\psi}_i | \nabla_{\mathbf{v}} | \psi_i \rangle \cdot \langle \bar{\psi}_j | \nabla_{\mathbf{v}} | \psi_j \rangle - \langle \bar{\psi}_i | \nabla_{\mathbf{v}} | \psi_j \rangle \cdot \langle \bar{\psi}_j | \nabla_{\mathbf{v}} | \psi_i \rangle \right). \end{aligned} \quad (\text{A5})$$

By solving the electronic equation of Eq. (A2), we can evaluate the NECSCF one-electron energy correction $\delta\varepsilon$,

$$\delta\varepsilon(\mathbf{R}) = \sum_i \langle \bar{\psi}_i | \hat{V}_{\chi}^{\text{cp}} | \psi_i \rangle. \quad (\text{A6})$$

The NECSCF energy correction $\delta E_{el}(\mathbf{R})$ is

$$\delta E_{el}(\mathbf{R}) = \sum_i \langle \bar{\psi}_i | \left(\hat{V}_{\chi}^{\text{cp}} + \frac{1}{2} \sum_{\mathbf{v}} \frac{1}{M_{\mathbf{v}}} \sum_j \langle \bar{\psi}_j | \nabla_{\mathbf{v}} \psi_j \rangle \cdot \nabla_{\mathbf{v}} - |\nabla_{\mathbf{v}} \psi_j \rangle \cdot \langle \bar{\psi}_j | \nabla_{\mathbf{v}} \right) | \psi_i \rangle. \quad (\text{A7})$$

Thus, the geometrically averaged NECSCF electronic energy E_{el} contains both contributions from the averaged BO electronic energy E_{BO} and the NECSCF correction,

$$E_{el} = \langle \chi | \hat{E}_{el}(\mathbf{R}) | \chi \rangle_{\mathbf{R}} = E_{BO} + \langle \chi | \delta E_{el}(\mathbf{R}) | \chi \rangle_{\mathbf{R}} \quad (\text{A8})$$

Next, we show that Eq. (A2), the NECSCF electronic equation, is form-invariant and independent of the gauge choice. To this end, we only need to show that the last two terms of the embedding operator $\hat{V}_{\chi}^{\text{cp}}$ are form-invariant, since only these terms are explicitly related to NECSCF MOs. Using the spectral representation $\hat{V}_{\chi}^{\text{cp}} = \sum_{pq} |\psi_p\rangle V_{\chi,pq}^{\text{cp}} \langle \bar{\psi}_q|$ in the complete NECSCF MOs, the last two terms of $\hat{V}_{\chi}^{\text{cp}}$ in Eq. (11) read

$$\begin{aligned} \sum_j \langle \bar{\psi}_j | \nabla_{\mathbf{v}} | \psi_j \rangle \cdot \nabla_{\mathbf{v}} &= \sum_{pq} |\psi_p\rangle \sum_j \langle \bar{\psi}_j | \nabla_{\mathbf{v}} | \psi_j \rangle \cdot \langle \bar{\psi}_p | \nabla_{\mathbf{v}} | \psi_q \rangle \langle \bar{\psi}_q | \\ &= \sum_{pq} |\psi_p\rangle \text{tr} \left(\mathbf{A}_{oo}^{(\mathbf{v})} \right) \cdot A_{pq}^{(\mathbf{v})} \langle \bar{\psi}_q |, \end{aligned} \quad (\text{A9})$$

$$\begin{aligned} \sum_j |\nabla_{\mathbf{v}} \psi_j \rangle \cdot \langle \bar{\psi}_j | \nabla_{\mathbf{v}} &= \sum_j \sum_{pq} |\psi_p\rangle \langle \bar{\psi}_p | \nabla_{\mathbf{v}} | \psi_j \rangle \cdot \langle \bar{\psi}_j | \nabla_{\mathbf{v}} | \psi_q \rangle \langle \bar{\psi}_q | \\ &= \sum_{pq} |\psi_p\rangle \sum_j A_{pj}^{(\mathbf{v})} \cdot A_{jq}^{(\mathbf{v})} \langle \bar{\psi}_q |. \end{aligned} \quad (\text{A10})$$

According to the unitary invariance given in Eqs. (C14) and (C15), these operators are form-invariant for a unitary transformation of NECSCF MOs. We can then pick NECSCF MOs that lead to a formal orbital energy $\varepsilon_i = \delta_{ij} \sum_{i'j'} T_{ii'}^* \tilde{\varepsilon}_{i'j'} T_{j'j}$ by a unitary transformation of the multipliers $\tilde{\varepsilon}_{ij}$.

Appendix B: Effective coupled equations

The nuclear equation (A3) indicates that the NECSCF electronic potential operator $\hat{E}_{el}(\mathbf{R})$ in Eq. (A5) yields a potential surface that depends on the nuclear wavefunction, unless the special gauge choice making $A_{ii}^{(v)} = 0$ is applied according to Eqs. (17) and (18). To better understand the nature of the coupled nuclear motion and associated energy surface, we define an effective geometric derivative $\tilde{\nabla}_v$ for the v -th vibration

$$\tilde{\nabla}_v = \nabla_v + \text{tr}(\mathbf{A}_{00}^{(v)}), \quad (\text{B1})$$

where the geometric derivative matrix $\mathbf{A}_{00}^{(v)}$ is composed of elements from the vector $\langle \bar{\psi}_i | \nabla_v | \psi_j \rangle$ for occupied MOs. The electronic equation is then converted to an equivalent form,

$$\left[\hat{F}_{\text{BO}} + \delta\varepsilon + \hat{V}_\chi^{\text{cp}} \right] |\psi_i\rangle = \frac{\varepsilon_i}{|\chi(\mathbf{R})|^2} |\psi_i\rangle, \quad (\text{B2})$$

with the effective embedding potential \hat{V}_χ^{cp}

$$\hat{V}_\chi^{\text{cp}} = -\sum_v \frac{1}{M_v} \left(\frac{\tilde{\nabla}_v \chi}{\chi} \cdot \tilde{\nabla}_v + \frac{\tilde{\nabla}_v^2}{2} - \sum_j |\tilde{\nabla}_v \psi_j\rangle \cdot \langle \bar{\psi}_j | \tilde{\nabla}_v \right), \quad (\text{B3})$$

and an orbital energy shift $\delta\varepsilon$,

$$\delta\varepsilon = \sum_v \frac{1}{M_v} \left[-\frac{1}{2} \text{tr}^2(\mathbf{A}_{00}^{(v)}) + \text{tr}(\mathbf{A}_{00}^{(v)}) \frac{\tilde{\nabla}_v \chi}{\chi} \right]. \quad (\text{B4})$$

Similarly, the effective nuclear equation is given by

$$\left[\hat{T}_n + \tilde{E}_{el}(\mathbf{R}) \right] \chi = E\chi \quad (\text{B5})$$

where the effective kinetic energy operator \hat{T}_n is

$$\hat{T}_n = -\sum_v \frac{\tilde{\nabla}_v^2}{2M_v} \quad (\text{B6})$$

and the effective electronic energy $\tilde{E}_{el}(\mathbf{R})$

$$\begin{aligned} \tilde{E}_{el}(\mathbf{R}) &= \langle \Phi(\mathbf{r}, \mathbf{R}) | \hat{H}_{\text{BO}} | \Phi(\mathbf{r}, \mathbf{R}) \rangle_{\mathbf{r}} + \sum_i \langle \bar{\psi}_i | \left(\delta\varepsilon + \hat{V}_\chi^{\text{cp}} - \frac{1}{2} \sum_v \frac{1}{M_v} \sum_j |\nabla_v \psi_j\rangle \cdot \langle \bar{\psi}_j | \nabla_v \right) | \psi_i \rangle \\ &= \langle \Phi(\mathbf{r}, \mathbf{R}) | \hat{H}_{\text{BO}} | \Phi(\mathbf{r}, \mathbf{R}) \rangle_{\mathbf{r}} - \sum_v \frac{1}{2M_v} \left(\sum_i \langle \bar{\psi}_i | \tilde{\nabla}_v^2 | \psi_i \rangle - \sum_{ij} \langle \bar{\psi}_i | \tilde{\nabla}_v | \psi_j \rangle \cdot \langle \bar{\psi}_j | \tilde{\nabla}_v | \psi_i \rangle \right) \end{aligned} \quad (\text{B7})$$

which is analogous to Eq. (A7). In deriving Eq. (B7), we note that the first term of $\delta\epsilon$ make no additive contribution to $\tilde{E}_{el}(\mathbf{R})$, and the third term compensates $-\frac{\tilde{\nabla}_v\chi}{\chi} \cdot \tilde{\nabla}_v$ from \hat{V}_χ^{cp} . It becomes clear that the nuclear motion carrying \hat{T}_n can be described on an effective electronic energy surface that is computed as the the NECSCF electronic energy correction.

Appendix C: Energy invariance to unitary rotation of NECSCF MOs

From the NECSCF energy correction $\delta E_{el}(\mathbf{R})$ in Eq. (A7), the NECSCF electronic energy contribution can be further formulated in tracing matrix,

$$\begin{aligned}\delta E_{el}(\mathbf{R}) &= -\sum_{\mathbf{v}} \frac{1}{M_{\mathbf{v}}} \left(\frac{\nabla_{\mathbf{v}}\chi}{\chi} \cdot A_{ii}^{(\mathbf{v})} + \frac{1}{2} \sum_a A_{ia}^{(\mathbf{v})} \cdot A_{ai}^{(\mathbf{v})} + \frac{1}{2} \nabla_{\mathbf{v}} \cdot A_{ii}^{(\mathbf{v})} \right) \\ &= -\sum_{\mathbf{v}} \frac{1}{2M_{\mathbf{v}}} \left(\frac{\nabla_{\mathbf{v}}\chi}{\chi} \text{tr}(\mathbf{A}_{oo}^{(\mathbf{v})}) + \text{tr}(\mathbf{A}_{ov}^{(\mathbf{v})} \mathbf{A}_{vo}^{(\mathbf{v})}) \right)\end{aligned}\quad (\text{C1})$$

We will show that all these terms lead to δE_{el} that is energy invariant to an unitary orbital rotation among all occupied MOs, regardless of the gauge choice. The matrices $\mathbf{A}_{oo}^{(\mathbf{v})}$, $\mathbf{A}_{ov}^{(\mathbf{v})}$ and $\mathbf{A}_{vo}^{(\mathbf{v})}$ collect the elements $A_{ij}^{(\mathbf{v})}$, $A_{ia}^{(\mathbf{v})}$ and $A_{ai}^{(\mathbf{v})}$, and are generically evaluated as follows, respectively,

$$\mathbf{A}_{oo}^{(\mathbf{v})} = \bar{\mathbf{C}}_o^\dagger \mathbf{S}^{0\mathbf{v}} \mathbf{C}_o + \mathbf{U}_{oo}^{(\mathbf{v})} \quad (\text{C2})$$

$$\mathbf{A}_{ov}^{(\mathbf{v})} = \bar{\mathbf{C}}_o^\dagger \mathbf{S}^{0\mathbf{v}} \mathbf{C}_v + \mathbf{U}_{ov}^{(\mathbf{v})} \quad (\text{C3})$$

$$\mathbf{A}_{vo}^{(\mathbf{v})} = \bar{\mathbf{C}}_v^\dagger \mathbf{S}^{0\mathbf{v}} \mathbf{C}_o + \mathbf{U}_{vo}^{(\mathbf{v})} \quad (\text{C4})$$

Consider the biorthogonal unitary transformations \mathbf{T}_{oo} and \mathbf{T}_{vv} among the occupied and virtual MOs at any molecular geometry \mathbf{R} , such that $\mathbf{T}_{oo} \bar{\mathbf{T}}_{oo}^\dagger = \mathbf{I}$ and $\mathbf{T}_{vv} \bar{\mathbf{T}}_{vv}^\dagger = \mathbf{I}$, respectively. The transformed MOs are

$$\mathbf{C}'_o = \mathbf{C}_o \mathbf{T}_{oo}, \quad (\text{C5})$$

$$\mathbf{C}'_v = \mathbf{C}_v \mathbf{T}_{vv}, \quad (\text{C6})$$

The geometrically perturbed (e.g., \mathbf{C}' and \mathbf{C}) and the unperturbed (e.g., $\mathbf{C}'^{(0)}$ and $\mathbf{C}^{(0)}$) MOs are related by,

$$\mathbf{C}'_o = \mathbf{C}'_o{}^{(0)} \mathbf{U}'_{oo} + \mathbf{C}'_v{}^{(0)} \mathbf{U}'_{vo}, \quad (\text{C7})$$

$$\mathbf{C}'_v = \mathbf{C}'_v{}^{(0)} \mathbf{U}'_{vv} + \mathbf{C}'_o{}^{(0)} \mathbf{U}'_{ov}. \quad (\text{C8})$$

$$\mathbf{C}_o = \mathbf{C}_o^{(0)} \mathbf{U}_{oo} + \mathbf{C}_v^{(0)} \mathbf{U}_{vo}, \quad (\text{C9})$$

$$\mathbf{C}_v = \mathbf{C}_v^{(0)} \mathbf{U}_{vv} + \mathbf{C}_o^{(0)} \mathbf{U}_{ov}. \quad (\text{C10})$$

Combining Eqs. (C5)–(C10) and noting that $\mathbf{U}_{oo}^{(0)} = \mathbf{U}_{vv}^{(0)} = \mathbf{I}$ and $\mathbf{U}_{ov}^{(0)} = \mathbf{U}_{vo}^{(0)} = 0$, we arrive at the following relations between the transformed and original relaxations,

$$\mathbf{U}'_{oo}{}^{(v)} = \mathbf{T}_{oo}^{\dagger(0)} \mathbf{U}_{oo}^{(v)} \mathbf{T}_{oo}^{(0)} + \left(\mathbf{T}_{oo}^{\dagger(0)} \mathbf{T}_{oo}^{(0)} \right)^{(v)} = \mathbf{T}_{oo}^{\dagger(0)} \mathbf{U}_{oo}^{(v)} \mathbf{T}_{oo}^{(0)}, \quad (\text{C11})$$

$$\mathbf{U}'_{ov}{}^{(v)} = \mathbf{T}_{oo}^{\dagger(0)} \mathbf{U}_{ov}^{(v)} \mathbf{T}_{vv}^{(0)}, \quad (\text{C12})$$

$$\mathbf{U}'_{vo}{}^{(v)} = \mathbf{T}_{vv}^{\dagger(0)} \mathbf{U}_{vo}^{(v)} \mathbf{T}_{oo}^{(0)}. \quad (\text{C13})$$

Now using the relations of Eqs. (C2) and C11, we can evaluate $\mathbf{A}'_{oo}{}^{(v)}$ and $\text{tr}(\mathbf{A}'_{oo}{}^{(v)})$,

$$\mathbf{A}'_{oo}{}^{(v)} = \bar{\mathbf{T}}_{oo}^{\dagger(0)} \mathbf{A}_{oo}^{(v)} \mathbf{T}_{oo}^{(0)} \quad (\text{C14})$$

$$\begin{aligned} \text{tr}(\mathbf{A}'_{oo}{}^{(v)}) &= \text{tr}(\bar{\mathbf{T}}_{oo}^{\dagger(0)} \mathbf{A}_{oo}^{(v)} \mathbf{T}_{oo}^{(0)}) \\ &= \text{tr}(\mathbf{A}_{oo}^{(v)} \mathbf{T}_{oo}^{(0)} \bar{\mathbf{T}}_{oo}^{\dagger(0)}) \\ &= \text{tr}\{\mathbf{A}_{oo}^{(v)}\}. \end{aligned} \quad (\text{C15})$$

It is obvious that $\text{tr}(\mathbf{A}'_{oo}{}^{(v)})$ is invariant regardless of the gauge choice.

For $\text{tr}(\mathbf{A}_{ov}^{(v)} \mathbf{A}_{vo}^{(v)})$, there is

$$\text{tr}(\mathbf{A}_{ov}^{(v)} \mathbf{A}_{vo}^{(v)}) = \text{tr}(\mathbf{S}^{0v} \mathbf{C}_v \bar{\mathbf{C}}_v^{\dagger} \mathbf{S}^{0v} \mathbf{C}_o \bar{\mathbf{C}}_o^{\dagger} + \mathbf{U}_{ov}^{(v)} \mathbf{U}_{vo}^{(v)} + \mathbf{S}^{0v} \mathbf{C}_v \mathbf{U}_{vo}^{(v)} \bar{\mathbf{C}}_o^{\dagger} + \mathbf{C}_o \mathbf{U}_{ov}^{(v)} \bar{\mathbf{C}}_v^{\dagger} \mathbf{S}^{0v}). \quad (\text{C16})$$

By referring to the relations in Eqs. (C5), (C6), (C12) and (C13), all the four terms are intrinsically invariant due to the unitarity of transformation matrices, which leads to

$$\text{tr}(\mathbf{A}'_{ov}{}^{(v)} \mathbf{A}'_{vo}{}^{(v)}) = \text{tr}(\mathbf{A}_{ov}^{(v)} \mathbf{A}_{vo}^{(v)}) \quad (\text{C17})$$

for any gauge transformation.

The invariance of the electronic potential leaves the formulation of nuclear equation in Eq. (10) invariant, i.e., both the total molecular energy and the nuclear density amplitudes on the same uniform grid set do not change. Therefore the occupied unitary \mathbf{T}_{oo} transforms the determinant wavefunction and the total wavefunction Ψ by a phase factor $\det(\mathbf{T}_{oo}) = e^{i\theta(\mathbf{R})}$,

$$\Phi' = \Phi \det(\mathbf{T}_{oo}), \quad (\text{C18})$$

$$\Psi' = \chi \Phi' = \det(\mathbf{T}_{oo}) \Psi = e^{i\theta(\mathbf{R})} \Psi. \quad (\text{C19})$$

Appendix D: Analytical first- and second-derivatives of FGH nuclear wavefunction

Assuming independent vibrational modes, we consider $\nabla_{\mathbf{v}}$ operator acting on a FGH vibrational wavefunction $\chi_{\mathbf{v}}$, leaving other vibrations frozen. The Fourier representation of the Dirac delta function is

$$\delta(\mathbf{R}'_{\mathbf{v}} - \mathbf{R}_{\mathbf{v}}) = \frac{1}{2\pi} \int_{-\infty}^{+\infty} e^{-ik(\mathbf{R}'_{\mathbf{v}} - \mathbf{R}_{\mathbf{v}})} dk \quad (\text{D1})$$

where the ranges of momentum space and position space are set to $-\infty \leq k \leq +\infty$ and $0 \leq \mathbf{R}_{\mathbf{v}} \leq +\infty$, respectively. Therefore,

$$\begin{aligned} \nabla_{\mathbf{v}} \chi_{\mathbf{v}} &= \frac{\partial}{\partial \mathbf{R}_{\mathbf{v}}} \int_0^{+\infty} \delta(\mathbf{R}'_{\mathbf{v}} - \mathbf{R}_{\mathbf{v}}) \chi'_{\mathbf{v}} d\mathbf{R}'_{\mathbf{v}} \\ &= \frac{\partial}{\partial \mathbf{R}_{\mathbf{v}}} \int_0^{+\infty} \left[\frac{1}{2\pi} \int_{-\infty}^{+\infty} e^{-ik(\mathbf{R}'_{\mathbf{v}} - \mathbf{R}_{\mathbf{v}})} dk \right] \chi'_{\mathbf{v}} d\mathbf{R}'_{\mathbf{v}} \\ &= \int_0^{+\infty} \left[\frac{1}{2\pi} \int_{-\infty}^{+\infty} ike^{-ik(\mathbf{R}'_{\mathbf{v}} - \mathbf{R}_{\mathbf{v}})} dk \right] \chi'_{\mathbf{v}} d\mathbf{R}'_{\mathbf{v}}. \end{aligned} \quad (\text{D2})$$

Both k and $\mathbf{R}_{\mathbf{v}}$ in Eq. (D2) are discretized on uniform grid points. Suppose the length of the coordinate grid is L and there are N grid points (N is odd), the spacings in the position and momentum grid are given by $\Delta \mathbf{R}_{\mathbf{v}} = \frac{L}{N}$ and $\Delta k = \frac{2\pi}{L}$.⁶² The values of k are evenly distributed around the origin of zero, ranging from $-n\Delta k$ to $n\Delta k$ with $n = \frac{N-1}{2}$. The details of the discretization process are available in ref. 63. Briefly, the matrix element of the first-order derivative operator over the internal coordinates (r_1, r_2) associated with the vibration $\chi_{\mathbf{v}}$ defined on this grid set can be written as

$$[\nabla_{\mathbf{v}}]_{r_1 r_2} = -\frac{4\pi}{LN} \sum_{k=1}^n k \sin \left[\frac{2\pi k(r_1 - r_2)}{N} \right]. \quad (\text{D3})$$

Obviously, the matrix for the first-derivative operator is anti-Hermitian. The sum in Eq. (D3) could be calculated analytically,

$$[\nabla_{\mathbf{v}}]_{r_1 r_2} = \begin{cases} 0 & \text{for } r_1 = r_2, \\ -\frac{2\pi}{LN} \left[\frac{\sin[(n+1)(r_1 - r_2) \frac{2\pi}{N}]}{2\sin^2[(r_1 - r_2) \frac{\pi}{N}]} + \frac{(-1)^{r_1 - r_2 + 1} (n+1)}{\sin[(r_1 - r_2) \frac{\pi}{N}]} \right] & \text{for } r_1 \neq r_2. \end{cases} \quad (\text{D4})$$

A similar derivation leads to the grid representation of the second-derivative operator,

$$[\nabla_{\mathbf{v}}^2]_{r_1 r_2} = \begin{cases} -\frac{4\pi^2}{L^2} \frac{n(n+1)}{3} & \text{for } r_1 = r_2, \\ -\frac{4\pi^2}{L^2} \frac{(-1)^{r_2 - r_1} (n+1) \cos[(r_2 - r_1) \frac{\pi}{N}] + (n+1) \cos[(n+1)(r_2 - r_1) \frac{2\pi}{N}] - \sin[(n+1)(r_2 - r_1) \frac{2\pi}{N}] \cot[(r_2 - r_1) \frac{\pi}{N}]}{2N \sin^2[(r_2 - r_1) \frac{\pi}{N}]} & \text{for } r_1 \neq r_2. \end{cases} \quad (\text{D5})$$

The analytical first- (or second-) derivative of FGH nuclear wavefunction is hence the matrix product between Eq. (D4) (or Eq. (D5)) with the grid representation of the nuclear wavefunction.

REFERENCES

- ¹M. Born and R. Oppenheimer, “Zur quantentheorie der molekeln,” *Ann. Phys.* **389**, 457–484 (1927).
- ²S. Hammes-Schiffer, “Theoretical perspectives on proton-coupled electron transfer reactions,” *Acc. Chem. Res.* **34**, 273–281 (2001).
- ³S. Hammes-Schiffer and A. V. Soudackov, “Proton-coupled electron transfer in solution, proteins, and electrochemistry,” *J. Phys. Chem. B* **112**, 14108–14123 (2008).
- ⁴S. Hammes-Schiffer and A. A. Stuchebrukhov, “Theory of coupled electron and proton transfer reactions,” *Chem. Rev.* **110**, 6939–6960 (2010).
- ⁵S. Hammes-Schiffer, “Proton-coupled electron transfer: classification scheme and guide to theoretical methods,” *Energy Environ. Sci.* **5**, 7696–7703 (2012).
- ⁶S. Hammes-Schiffer, “Proton-coupled electron transfer: moving together and charging forward,” *J. Am. Chem. Soc.* **137**, 8860–8871 (2015).
- ⁷M. Ashfold, B. Cronin, A. Devine, R. Dixon, and M. Nix, “The role of $\pi\sigma^*$ excited states in the photodissociation of heteroaromatic molecules,” *Science* **312**, 1637–1640 (2006).
- ⁸G. M. Roberts, A. S. Chatterley, J. D. Young, and V. G. Stavros, “Direct observation of hydrogen tunneling dynamics in photoexcited phenol,” *J. Phys. Chem. Lett.* **3**, 348–352 (2012).
- ⁹C. Xie, J. Ma, X. Zhu, D. R. Yarkony, D. Xie, and H. Guo, “Nonadiabatic tunneling in photodissociation of phenol,” *J. Am. Chem. Soc.* **138**, 7828–7831 (2016).
- ¹⁰T. Yonehara, K. Hanasaki, and K. Takasuka, “Fundamental approaches to nonadiabaticity: Toward a chemical theory beyond the born–oppenheimer paradigm,” *Chem. Rev.* **112**, 499–542 (2012).
- ¹¹S. Habershon, D. E. Manolopoulos, T. E. Markland, and T. F. Miller, “Ring-polymer molecular dynamics: Quantum effects in chemical dynamics from classical trajectories in an extended phase space,” *Annu. Rev. Phys. Chem.* **64**, 387–413 (2013).
- ¹²B. F. E. Curchod and T. J. Martínez, “Ab initio nonadiabatic quantum molecular dynamics,” *Chem. Rev.* **118**, 3305–3336 (2018).
- ¹³S. Garashchuk, J. C. Light, and V. A. Rassolov, “The diagonal born–oppenheimer correction to molecular dynamical properties,” *Chem. Phys. Lett.* **333**, 459–464 (2001).
- ¹⁴E. F. Valeev and C. D. Sherrill, “The diagonal born–oppenheimer correction beyond the hartree–fock approximation,” *J. Chem. Phys.* **118**, 3921–3927 (2003).

- ¹⁵H.-D. Meyer, U. Manthe, and L. S. Cederbaum, “The multi-configurational time-dependent hartree approach,” *Chem. Phys. Lett.* **15**, 73–78 (1990).
- ¹⁶M. Beck, A. Jäckle, G. Worth, and H.-D. Meyer, “The multiconfiguration time-dependent hartree (mctdh) method: a highly efficient algorithm for propagating wavepackets,” *Phys. Rep.* **324**, 1–105 (2000).
- ¹⁷P. M. Kozłowski and L. Adamowicz, “Equivalent quantum approach to nuclei and electrons in molecules,” *Chem. Rev.* **93**, 2007–2022 (1993).
- ¹⁸N. M. Tubman, I. Kylänpää, S. Hammes-Schiffer, and D. M. Ceperley, “Beyond the born-oppenheimer approximation with quantum monte carlo methods,” *Phys. Rev. A* **90**, 042507 (2014).
- ¹⁹Y. Yang, I. Kylänpää, N. M. Tubman, J. T. Krogel, S. Hammes-Schiffer, and D. M. Ceperley, “How large are nonadiabatic effects in atomic and diatomic systems?” *J. Chem. Phys.* **143**, 124308 (2015).
- ²⁰H. Nishizawa, M. Hoshino, Y. Imamura, and H. Nakai, “Evaluation of electron repulsion integral of the explicitly correlated gaussian-nuclear orbital plus molecular orbital theory,” *Chem. Phys. Lett.* **521**, 142–149 (2012).
- ²¹I. L. Thomas, “Protonic structure of molecules. i. ammonia molecules.” *Phys. Rev.* **185**, 90–94 (1969).
- ²²I. L. Thomas, “The protonic structure of methane, ammonia, water, and hydrogen fluoride.” *Chem. Phys. Lett.* **3**, 705–706 (1969).
- ²³I. L. Thomas and H. W. Joy, “Protonic structure of molecules. ii. methodology, center-of-mass transformation, and the structure of methane, ammonia, and water.” *Phys. Rev. A* **2**, 1200–1208 (1970).
- ²⁴M. Tachikawa, K. Mori, H. Nakai, and K. Iguchi, “An extension of ab initio molecular orbital theory to nuclear motion.” *Chem. Phys. Lett.* **290**, 437–442 (1998).
- ²⁵M. Tachikawa and Y. Osamura, “Isotope effect of hydrogen and lithium hydride molecules. application of the dynamic extended molecular orbital method and energy component analysis,” *Theor. Chem. Acc.* **104**, 29–39 (2000).
- ²⁶M. Tachikawa, “Multi-component molecular orbital theory for electrons and nuclei including many-body effect with full configuration interaction treatment: Isotope effects on hydrogen molecules,” *Chem. Phys. Lett.* **360**, 494–500 (2002).
- ²⁷H. Nakai and K. Sodeyama, “Many-body effects in nonadiabatic molecular theory for simul-

- taneous determination of nuclear and electronic wave functions: Ab initio nomo/mbpt and cc methods,” *J. Chem. Phys.* **118**, 1119–1127 (2003).
- ²⁸A. D. Bochevarov, E. F. Valeev, and C. D. Sherrill, “The electron and nuclear orbitals model: Current challenges and future prospects.” *Mol. Phys.* **102**, 111–123 (2004).
- ²⁹T. Ishimoto, M. Tachikawa, and U. Nagashima, “Review of multicomponent molecular orbital method for direct treatment of nuclear quantum effect,” *Int. J. Quantum Chem.* **109**, 2677–2694 (2009).
- ³⁰H. Nakai, “Nuclear orbital plus molecular orbital theory: Simultaneous determination of nuclear and electronic wave functions without born–oppenheimer approximation,” *Int. J. Quantum Chem.* **107**, 2849–2869 (2007).
- ³¹F. Pavošević, T. Culpitt, and S. Hammes-Schiffer, “Multicomponent quantum chemistry: Integrating electronic and nuclear quantum effects via the nuclear–electronic orbital method,” *Chem. Rev.* **120**, 4222–4253 (2020).
- ³²A. Chakraborty, M. V. Pak, and S. Hammes-Schiffer, “Development of electron-proton density functionals for multicomponent density functional theory,” *Phys. Rev. Lett.* **101**, 153001 (2008).
- ³³K. R. Brorsen, Y. Yang, and S. Hammes-Schiffer, “Multicomponent density functional theory: Impact of nuclear quantum effects on proton affinities and geometries,” *J. Phys. Chem. Lett.* **8**, 3488–3493 (2017).
- ³⁴F. Pavošević, B. J. Rousseau, and S. Hammes-Schiffer, “Multicomponent orbital-optimized perturbation theory methods: Approaching coupled cluster accuracy at lower cost,” *J. Phys. Chem. Lett.* **11**, 1578–1583 (2020).
- ³⁵Q. Yu and S. Hammes-Schiffer, “Nuclear-electronic orbital multistate density functional theory,” *J. Phys. Chem. Lett.* **11**, 10106–10113 (2020).
- ³⁶Y. Yang, K. R. Brorsen, T. Culpitt, M. V. Pak, and S. Hammes-Schiffer, “Development of a practical multicomponent density functional for electron-proton correlation to produce accurate proton densities,” *J. Chem. Phys.* **147**, 114113 (2017).
- ³⁷X. Xu and Y. Yang, “Full-quantum descriptions of molecular systems from constrained nuclear–electronic orbital density functional theory,” *J. Chem. Phys.* **153**, 074106 (2020).
- ³⁸X. Xu and Y. Yang, “Constrained nuclear-electronic orbital density functional theory: Energy surfaces with nuclear quantum effects,” *J. Chem. Phys.* **152**, 084107 (2020).
- ³⁹X. Xu and Y. Yang, “Molecular vibrational frequencies from analytic hessian of constrained nuclear–electronic orbital density functional theory,” *J. Chem. Phys.* **154**, 244110 (2021).

- ⁴⁰Y. Yang, T. Culpitt, and S. Hammes-Schiffer, “Multicomponent time-dependent density functional theory: Proton and electron excitation energies,” *J. Phys. Chem. Lett.* **9**, 1765–1770 (2018).
- ⁴¹T. Culpitt, Y. Yang, F. Pavošević, Z. Tao, and S. Hammes-Schiffer, “Enhancing the applicability of multicomponent time-dependent density functional theory,” *J. Chem. Phys.* **150**, 201101 (2019).
- ⁴²F. Pavošević, Z. Tao, and S. Hammes-Schiffer, “Multicomponent coupled cluster singles and doubles with density fitting: Protonated water tetramers with quantized protons,” *J. Phys. Chem. Lett.* **12**, 1631–1637 (2021).
- ⁴³S. P. Webb, T. Jordanov, and S. Hammes-Schiffer, “Multiconfigurational nuclear-electronic orbital approach: Incorporation of nuclear quantum effects in electronic structure calculations,” *J. Chem. Phys.* **117**, 4106–4118 (2002).
- ⁴⁴K. R. Brorsen, “Quantifying multireference character in multicomponent systems with heat-bath configuration interaction,” *J. Chem. Theory Comput.* **16**, 2379–2388 (2020).
- ⁴⁵O. J. Fajen and K. R. Brorsen, “Separation of electron–electron and electron–proton correlation in multicomponent orbital-optimized perturbation theory,” *J. Chem. Phys.* **152**, 194107 (2020).
- ⁴⁶O. J. Fajen and K. R. Brorsen, “Multicomponent casscf revisited: Large active spaces are needed for qualitatively accurate protonic densities,” *J. Chem. Theory Comput.* **17**, 965–974 (2021).
- ⁴⁷G. Hunter, “Conditional probability amplitudes in wave mechanics,” *Int. J. Quantum Chem.* **9**, 237–242 (1975).
- ⁴⁸L. S. Cederbaum, “The exact molecular wavefunction as a product of an electronic and a nuclear wavefunction,” *J. Chem. Phys.* **138**, 224110 (2013).
- ⁴⁹L. S. Cederbaum, “Erratum:”the exact molecular wavefunction as a product of an electronic and a nuclear wavefunction” [*j. chem. phys.* 138, 224110 (2013)],” *J. Chem. Phys.* **141**, 029902 (2014).
- ⁵⁰N. I. Gidopoulos and E. K. U. Gross, “Electronic non-adiabatic states: towards a density functional theory beyond the born–oppenheimer approximation,” *Philos. Trans. R. Soc. A* **372**, 20130059 (2014).
- ⁵¹R. Requist and E. Gross, “Exact factorization-based density functional theory of electrons and nuclei,” *Phys. Rev. Lett.* **117**, 193001 (2016).
- ⁵²C. Li, R. Requist, and E. Gross, “Density functional theory of electron transfer beyond the born–oppenheimer approximation: Case study of lif,” *J. Chem. Phys.* **148**, 084110 (2018).

- ⁵³A. Abedi, N. T. Maitra, and E. K. U. Gross, “Exact factorization of the time-dependent electron-nuclear wave function,” *Phys. Rev. Lett.* **105**, 123002 (2010).
- ⁵⁴A. Abedi, N. T. Maitra, and E. K. U. Gross, “Correlated electron-nuclear dynamics: Exact factorization of the molecular wavefunction,” *J. Chem. Phys.* **137**, 22A530 (2012).
- ⁵⁵Y.-C. Chiang, S. Klaiman, and L. S. Cederbaum, “The exact wavefunction factorization of a vibronic coupling system,” *J. Chem. Phys.* **140**, 054104 (2014).
- ⁵⁶F. Agostini, A. Abedi, and E. K. U. Gross, “Classical nuclear motion coupled to electronic non-adiabatic transitions,” *J. Chem. Phys.* **141**, 214101 (2014).
- ⁵⁷S. K. Min, F. Agostini, I. Tavernelli, and E. K. U. Gross, “Ab initio nonadiabatic dynamics with coupled trajectories: A rigorous approach to quantum (de)coherence,” *J. Phys. Chem. Lett.* **8**, 3048–3055 (2017).
- ⁵⁸G. H. Gossel, L. Lacombe, and N. T. Maitra, “On the numerical solution of the exact factorization equations,” *J. Chem. Phys.* **150**, 154112 (2019).
- ⁵⁹M. Sibaev, I. Polyak, F. R. Manby, and P. J. Knowles, “Molecular second-quantized hamiltonian: Electron correlation and non-adiabatic coupling treated on an equal footing,” *J. Chem. Phys.* **153**, 124102 (2020).
- ⁶⁰H. Sellers and P. Pulay, “The adiabatic correction to molecular potential surfaces in the scf approximation,” *Chem. Phys. Lett.* **103**, 463–465 (1984).
- ⁶¹O. Rosas-Ortiz and K. Zelaya, “Bi-orthogonal approach to non-hermitian hamiltonians with the oscillator spectrum: generalized coherent states for nonlinear algebras,” *Annals of Physics* **388**, 26–53 (2018).
- ⁶²C. C. Marston and G. G. Balint-Kurti, “The fourier grid hamiltonian method for bound state eigenvalues and eigenfunctions,” *J. Chem. Phys.* **91**, 3571–3576 (1989).
- ⁶³J. Stare and G. G. Balint-Kurti, “Fourier grid hamiltonian method for solving the vibrational schrödinger equation in internal coordinates: Theory and test applications,” *J. Phys. Chem. A* **107**, 7204–7214 (2003).
- ⁶⁴J. Czub and L. Wolniewicz, “On the non-adiabatic potentials in diatomic molecules,” *Mol. Phys.* **36**, 1301–1308 (1978).
- ⁶⁵Q. Sun, X. Zhang, S. Banerjee, P. Bao, M. Barbry, N. S. Blunt, N. A. Bogdanov, G. H. Booth, J. Chen, Z. Cui, J. J. Eriksen, Y. Gao, S. Guo, J. Hermann, M. R. Hermes, K. Koh, P. Koval, S. Lehtola, Z. Li, J. Liu, N. Mardirossian, J. D. McClain, M. Motta, B. Mussard, H. Q. Pham, A. Pulkin, W. Purwanto, P. J. Robinson, E. Ronca, E. Sayfutyarova, M. Scheurer, H. F. Schurkus,

- J. E. T. Smith, C. Sun, S. Sun, S. Upadhyay, L. K. Wagner, X. Wang, A. White, J. D. Whitfield, M. J. Williamson, S. Wouters, J. Yang, J. M. Yu, T. Zhu, T. C. Berkelbach, S. Sharma, A. Y. Sokolov, and G. K.-L. Chan, "Recent developments in the pyscf program package," *J. Chem. Phys.* **153**, 024109 (2020).
- ⁶⁶I. G. Ryabinkin, L. Joubert-Doriol, and A. F. Izmaylov, "Geometric Phase Effects in Nonadiabatic Dynamics near Conical Intersections," *Acc. Chem. Res.* **50**, 1785–1793 (2017).
- ⁶⁷L. Hilico, N. Billy, B. Grémaud, and D. Delande, "Ab initio calculation of the $j = 0$ and $j = 1$ states of the h_2^+ , d_2^+ and hd^+ molecular ions." *Eur. Phys. J. D* **12**, 449–466 (2000).
- ⁶⁸D. M. Bishop, "Non-adiabatic calculations for h_2^+ , hd^+ and d_2^+ ," *Mol. Phys.* **28**, 1397–1408 (1974).
- ⁶⁹S. Alexander and R. Coldwell, "Vibrational energies of h_2^+ using fully nonadiabatic wavefunctions," *Int. J. Quantum Chem.* **112**, 3703–3705 (2012).
- ⁷⁰T. Helgaker, W. Klopper, H. Koch, and J. Noga, "Basis-set convergence of correlated calculations on water," *J. Chem. Phys.* **106**, 9639–9646 (1997).
- ⁷¹F. N. N. Pansini, A. C. Neto, and A. J. C. Varandas, "Extrapolation of hartree–fock and multi-configuration self-consistent-field energies to the complete basis set limit," *Theor. Chem. Acc.* **135**, 261 (2016).
- ⁷²L. Wolniewicz, "Nonadiabatic energies of the ground state of the hydrogen molecule," *J. Chem. Phys.* **103**, 1792–1799 (1995).
- ⁷³S. Bubin, F. Leonarski, M. Stanke, and L. Adamowicz, "Non-adiabatic corrections to the energies of the pure vibrational states of h_2 ," *Chem. Phys. Lett.* **477**, 12–16 (2009).
- ⁷⁴E. P. L. Hunter and S. G. Lias, "Evaluated gas phase basicities and proton affinities of molecules: An update." *J. Phys. Chem. Ref. Data* **27**, 413–656 (1998).
- ⁷⁵C. C. Costain, "Determination of molecular structures from ground state rotational constants." *J. Chem. Phys.* **29**, 864–874 (1958).
- ⁷⁶M. Hargittai and I. Hargittai, "Experimental and computed bond lengths: The importance of their differences." *Int. J. Quantum Chem.* **44**, 1057–1067 (1992).
- ⁷⁷R. D. I. Johnson, NIST Computational Chemistry Comparison and Benchmark Database. , <http://cccbdb.nist.gov/> (accessed January 2021) (2021).
- ⁷⁸A. Tachibana, K. Hori, Y. Asai, and T. Yamabe, "Dynamic analysis of electron density in the course of the internal motion of molecular system," *J. Chem. Phys.* **80**, 6170–6178 (1984).
- ⁷⁹K. R. Brorsen, P. E. Schneider, and S. Hammes-Schiffer, "Alternative forms and transferability

- of electron-proton correlation functionals in nuclear-electronic orbital density functional theory,” *J. Chem. Phys.* **149**, 044110 (2018).
- ⁸⁰M. Moshinsky and C. Kittel, “How good is the born-oppenheimer approximation?” *Proc. Natl. Acad. Sci. U.S.A.* **60**, 1110–1113 (1968).
- ⁸¹M. Puchalski, A. Spyszkiewicz, J. Komasa, and K. Pachucki, “Nonadiabatic relativistic correction to the dissociation energy of h_2 , d_2 , and hd .” *Phys. Rev. Lett.* **121**, 073001 (2018).
- ⁸²F. Pawłowski, P. Jørgensen, J. Olsen, F. Hegelund, T. Helgaker, J. Gauss, K. L. Bak, and J. F. Stanton, “Molecular equilibrium structures from experimental rotational constants and calculated vibration–rotation interaction constants.” *J. Chem. Phys.* **116**, 6482–6496 (2002).